Robust Optimal Output-tracking Control of Constrained Mechanical Systems with Application to Autonomous Rovers

Mohammadreza Mottaghi, Robin Chhabra, *Member, IEEE*

***Abstract*— This paper presents a robust optimal output-tracking control strategy for underactuated mechanical systems whose motion is restricted by mixed holonomic and nonholonomic constraints. Autonomous rovers/cars and unmanned underwater/aerial vehicles are a few examples of such systems that must often operate in harsh environments and under uncertain conditions. We present a comprehensive control analysis of this large class of nonlinear systems, including the existing studies on local reachability and static state feedback linearization. We also propose a local observability analysis of the feedback transformed input-output linearized systems. Based on the input-output linearization of the holonomically restricted nominal system, we develop a sliding mode control strategy that is robust against projected effects of uncertainties and disturbances on the system's output. Asymptotic stability of the output towards a bounded desired trajectory is proved using Lyapunov's direct method while the system's internal stability (in the sense of boundedness) is investigated based on the notion of tracking-error zero dynamics. Time-dependent bounded matched uncertainties in the inertia parameters and disturbance forces arising in the unrestricted system are considered in this study. We propose an optimal sliding manifold according to the finite-horizon linear-quadratic regulator design problem with split boundary value conditions. The developed control strategy is implemented on a six-wheel autonomous Lunar rover in a simulation environment and its performance is compared with that of an optimal proportional-integral-derivative feedback, feedforward controller. The optimal sliding mode controller shows superior performance in trajectory tracking with acceptable control actions.**

***Index Terms*— Robust Output-tracking, Feedback Linearization, Nonholonomic Mechanics, Sliding Mode Control, Optimal Control.**

I. Introduction

CONSTRAINED robotic systems play a central role in many modern applications, such as space exploration, search and rescue, and aerial package delivery. Such systems inherent complex dynamics and due to their mission requirements they must operate autonomously under uncertain and hostile conditions. Thus, robustness is a crucial factor that should be considered in the design of their control systems.

Presence of constraints in mechanical systems, particularly nonholonomic (non-integrable) ones, introduces modelling and control challenges, e.g., underactuation and loss of full-state feedback linearizability property [1]. Several comprehensive frameworks have been presented to capture the behaviour of mechanical systems with constraints, specially in Pfaffian form [2], [3]. In [4], a unified dynamical model of robotic systems subject to nonlinear constraints is outlined that is based on differential variational principles. Yun and Sarkar unify the state space representation of systems subject to mixed holonomic (integrable) and nonholonomic constraints via substituting algebraic holonomic equations by stable first-order differential equations to improve the stability of numerical simulations [5]. Control challenges associated with nonholonomic systems, such as motion planning and feedback stabilization, are well-documented in the literature [6], [7]. A geometric exposition on nonholonomic control is presented in a book by Bloch that includes studying symmetry properties, optimal control and energy-based methods of stabilization of nonholonomic systems [8]. An optimal point stabilization control of nonholonomic systems is proposed based on an affine connection formulation [9]. Trajectory stabilization of nonholonomic systems has been also addressed using, e.g., a linearized model of system around a trajectory [10] or applying optimal control theory and Pontryagin maximum principle [11]. Further, output-tracking control laws for mechanical systems with nonholonomic rolling constraints have been developed based on input-output linearization techniques [12]. Chhabra *et al.* propose an output-tracking control strategy for symmetric nonholonomic Hamiltonian systems [13], founded upon their dynamical reduction [14] and input-output linearization in their reduced state space, applying static state feedback. This technique is implemented to design a torque-based controller for the Lunar Exploration Light Rover [15].

In reference to robust control of nonlinear systems, various techniques including integral control, Sliding Mode Control (SMC), and gain scheduling are discussed in a book by Khalil [16]. Nonlinear robust controllers can be also designed applying exogenous disturbance observers and adaptive control laws under the assumption that the uncertain dynamics can be estimated [17], [18]. Sliding mode control, as a robust variable structure control strategy, has been employed in many control applications, due to its simple structure, guaranteed asymptotic stability, and introduction of reduced order error dynamics [19]. To improve the performance of SMC, a chattering-free SMC is derived based on a time varying feedback gain, whose global stability is proven using the Lyapunov second theorem

M.R. Mottaghi and R. Chhabra are with the Mechanical and Aerospace Engineering department, Carleton University, Ottawa, Canada (e-mail: mohammadreza.mottaghi@carleton.ca, robin.chhabra@carleton.ca

and invariance principle [20]. In [21] using output feedback and applying SMC to the input-output dynamics, a robust output tracking control law is proposed along with a time-dependant exponent parameter law to ensure both accuracy and low energy consumption. Ge *et al.* propose a robust adaptive state/output feedback point stabilization of a class of nonholonomic systems in chained form along with an adaptive switching law guaranteeing the boundedness of the states [22]. For systems subject to holonomic and nonholonomic constraints, a systematic robust motion/force control law is developed based on an online adaptive parameter estimation [23]. A robust control scheme has also been developed for stabilization of nonholonomic systems with drift uncertainties, using time-varying SMC [24].

A category of mechanical systems that are subject to both holonomic and nonholonomic constraints is autonomous planetary exploration rovers that often experience several forms of uncertainties and disturbances [25]. The evolution of control systems developed for nonholonomic rovers initiated in 1990s. The full posture kinematic tracking control of Differential Drive Rovers (DDRs), based on Lyapunov design, is proposed in [26]. This result was extended to include robustness by designing a SMC in polar coordinates for DDRs experiencing unknown disturbing forces [27]. Ashrafiuon *et al.* develop a SMC for uncertain simple planar vehicles with only two control inputs that is robust against bounded time-dependant matched uncertainties. This method is based on a reduced order error dynamics obtained using the concept of transitional trajectory [28]. State feedback linearization of different types of rover systems has been also investigated, applying static or dynamic state feedback [29]. Wang and Xu propose a set of output functions for which rover systems are input-output linearizable applying static state feedback [30].

This paper presents a complete control analysis for a class of constrained mechanical systems that are subject to both holonomic and nonholonomic constraints in Pfaffian form. We extend the local reachability investigation discussed in [31] to general constrained systems, and collect different analyses on feedback linearizability and output-tracking control performed in [16], [30]–[32]. Additionally, we investigate the observability properties of such systems after applying an input-output linearizing feedback transformation. The main objective of this paper is to develop a robust optimal output-tracking control strategy for this class of mechanical systems, by input-output linearizing the nominal plant. Time-dependent matched uncertainties in inertia parameters and disturbance forces arising in the unrestricted dynamics of the system are considered. We propose a SMC with an optimally designed sliding manifold to increase the robustness of the output-tracking control task against projected effects of uncertainties and disturbances on the system's output. We obtain the sliding manifold by solving a Linear-Quadratic Regulator (LQR) design problem with split boundary value conditions. The error dynamics on the optimal sliding manifold follows a Proportional-Integral-Derivative (PID) control law, whose integral term also helps with the robustness of the system. Using the Lyapunov's direct method, we prove the asymptotic stability of the output error towards the origin. Further, we show the asymptotic stability of the observable internal states and boundedness of the unobservable internal states applying the concept of tracking-error zero dynamics. To alleviate the chattering effects associated with the developed SMC, we used the method of boundary layer proposed in [16], [33] and substitute the sign function in the switching control law by a high-slope continuous saturation function. The major contributions of this paper are as follows:

(i) We propose an observability decomposition of the internal states of constrained mechanical control systems that is used in the stability analysis of the internal dynamics.
(ii) We develop a robust output-tracking SMC strategy that is applicable to a wide range of constrained mechanical systems experiencing complex bounded time-dependent matched uncertainties in their inertia parameters.
(iii) We design an optimal sliding manifold at the output level that minimizes a functional based on a norm square of the output error and that of the control actions.

The developed control strategy is implemented on a six-wheel type $(1,1)$ autonomous rover that is designed for future Lunar exploration missions. Uncertainties in the form of added moving mass, variable moment of inertia, unbalanced wheel, and time-varying external forces are considered in the control design of the rover. We demonstrate the efficacy of the proposed optimal SMC thorough showing its superior performance in comparison to that of an optimally designed output-tracking PID feedback, feedforward controller. Note that the results of this paper can be directly applied to robotic systems, including autonomous cars and underwater/aerial vehicles, with 2- dimensional planar mobility.

The outline of the paper is as follows. Section II discusses the dynamical modelling of constrained mechanical systems with both holonomic and nonholonomic constraints. In Section III, various control aspects and state decompositions of constrained mechanical systems are studied. The proposed optimal robust output-tracking control algorithm is detailed in Section IV. Finally, the developed theory is implemented on a six-wheel autonomous Lunar rover in section V. Section VI provides some concluding remarks.

II. Constrained Mechanical Systems

In this section, we describe a class of mechanical control systems with mixed holonomic and nonholonomic constraints. We consider the evolution of such systems in the tangent bundle of their $\hat{n}$-dimensional smooth configuration manifold, denoted by $\hat{Q}$. A set of r everywhere linearly independent constraints on velocities in Pfaffian form is considered:

$$\hat{A}(\hat{\mathbf{q}})\dot{\hat{\mathbf{q}}} = 0, \tag{1}$$

where $(\hat{\mathbf{q}}, \dot{\hat{\mathbf{q}}}) \in T\hat{Q}$, the tangent bundle of the configuration manifold, and $\hat{A} : \hat{Q} \to \mathbb{R}^{r\times\hat{n}}$ is the constraint matrix. All admissible velocities of the system must lie in the $(\hat{n}-r)$-dimensional annihilator distribution $\mathcal{D}$ resulted from the constraint equations. Let $\hat{N} : \hat{Q} \to \mathbb{R}^{\hat{n}\times(\hat{n}-r)}$ denote the matrix whose columns span $\mathcal{D}$, i.e., $\hat{A}(\hat{\mathbf{q}})\hat{N}(\hat{\mathbf{q}}) = 0$.

Assumption 1. We assume that there exists a choice of $\hat{N}$ which is everywhere full-rank on $\hat{Q}$.

Based on the Lagrange d'Alembert principle, dynamics of the constrained mechanical system is derived in matrix form:

$$\begin{aligned} \hat{A}(\hat{\mathbf{q}})\dot{\hat{\mathbf{q}}} &= 0, \\ \hat{M}(\hat{\mathbf{q}})\ddot{\hat{\mathbf{q}}} + \hat{C}(\hat{\mathbf{q}},\dot{\hat{\mathbf{q}}})\dot{\hat{\mathbf{q}}} + \hat{\mathbf{g}}(\hat{\mathbf{q}}) &= \hat{B}(\hat{\mathbf{q}})\boldsymbol{\tau} + \hat{A}(\hat{\mathbf{q}})^T\hat{\boldsymbol{\lambda}}, \end{aligned} \tag{2}$$

where $\hat{M} : \hat{Q} \to \mathbb{R}^{\hat{n}\times\hat{n}}$ is the symmetric positive definite mass matrix of the system, $\hat{C} : T\hat{Q} \to \mathbb{R}^{\hat{n}\times\hat{n}}$ is the matrix of Coriolis and centrifugal forces, $\hat{\mathbf{g}} : \hat{Q} \to \mathbb{R}^{\hat{n}}$ is the vector of potential forces, $\boldsymbol{\tau} \in \mathbb{R}^s$ is the vector of control inputs, $\hat{B} : \hat{Q} \to \mathbb{R}^{\hat{n}\times s}$ is the matrix whose columns are the control directions, and $\hat{\boldsymbol{\lambda}} \in \mathbb{R}^r$ is the vector of Lagrange multipliers. Hereinafter, for brevity the dependency of the matrices and vectors is dropped wherever it does not raise confusion.

Assumption 2. The dimension of the vector $\boldsymbol{\tau}$ is greater than or equal to the dimension of distribution $\mathcal{D}$, i.e., $s \geq \hat{n} - r$, and no columns of $\hat{B}$ are in the image of $\hat{A}$.

If the involutive closure of $\mathcal{D}$, denoted by $\bar{\mathcal{D}}$, is of system's dimension ($\hat{n}$), then all imposed constraints are nonholonomic (non-integrable). The involutive closure of $\mathcal{D}$ is the minimal distribution that contains elements of $\mathcal{D}$ and all iterative Lie-brackets of vector fields in $\mathcal{D}$. If the dimension of $\bar{\mathcal{D}}$ is equal to $n = \hat{n} - p$, the system experiences p holonomic (integrable) constraints and $m = r - p$ nonholonomic constraints.

After identifying the holonomic constraints, we introduce the restricted configuration manifold Q, with dimension n, which is an embedded sub-manifold of $\hat{Q}$ with the inclusion map $\iota_Q : Q \to \hat{Q}$. In other words, Q is the maximal integral manifold of the holonomic distribution. Let $(\mathbf{q}, \dot{\mathbf{q}}) \in TQ$ denote an element of the tangent bundle of Q, and let $J(\mathbf{q})$ be the Jacobian of the inclusion map. The set of m remaining completely nonholonomic constraints on Q are defined by:

$$A(\mathbf{q})\dot{\mathbf{q}} = 0, \tag{3}$$

where

$$A(\mathbf{q}) = E\hat{A}(\iota_Q(\mathbf{q}))J(\mathbf{q}). \tag{4}$$

Due to inclusion of holonomic constraints, the rows of the matrix $\hat{A}J$ are linearly dependant and they span a co-distribution of dimension m. Here, the constant matrix $E \in \mathbb{R}^{m\times r}$ introduces a minimal linear combination of the rows of $\hat{A}J$ to parameterize the resultant co-distribution, which eliminates the redundant constraint directions.

Pre-multiplying both sides of (2) by $J^T(\mathbf{q})$, and substituting $\dot{\hat{\mathbf{q}}}$ and $\ddot{\hat{\mathbf{q}}}$, based on the inclusion map, i.e.,

$$\begin{aligned} \dot{\hat{\mathbf{q}}} &= J(\mathbf{q})\dot{\mathbf{q}}, \\ \ddot{\hat{\mathbf{q}}} &= \dot{J}(\mathbf{q},\dot{\mathbf{q}})\dot{\mathbf{q}} + J(\mathbf{q})\ddot{\mathbf{q}}, \end{aligned} \tag{5}$$

where

$$\dot{J}(\mathbf{q},\dot{\mathbf{q}}) = \sum_{j=1}^{n} \frac{\partial J(\mathbf{q})}{\partial \mathbf{q}_j}\dot{\mathbf{q}}_j,$$

is the time derivative of the matrix J, the equations of motion in the restricted configuration manifold Q become:

$$\begin{aligned} \dot{\mathbf{q}} &= N(\mathbf{q})\boldsymbol{\eta}, \\ M(\mathbf{q})\ddot{\mathbf{q}} + C(\mathbf{q},\dot{\mathbf{q}})\dot{\mathbf{q}} + \mathbf{g}(\mathbf{q}) &= B(\mathbf{q})\boldsymbol{\tau} + A(\mathbf{q})^T\boldsymbol{\lambda}. \end{aligned} \tag{6}$$

Here, $\mathbf{q}_j$ denotes the j^{th} element of $\mathbf{q}$, $N : Q \to \mathbb{R}^{n\times n-m}$ is a matrix whose columns span the null-space of the constraint matrix A (The existence of everywhere full-rank matrix N can be directly deduced from Assumption 1 and the fact that Q is an embedded submanifold of $\hat{Q}$), and $\boldsymbol{\eta} \in \mathbb{R}^{n-m}$ is the vector of quasi-velocities, $M := J^T\hat{M}(\iota_Q(\mathbf{q}))J$ is the mass matrix, $C := J^T(\hat{M}(\iota_Q(\mathbf{q}))\dot{J} + \hat{C}(\iota_Q(\mathbf{q}), J\dot{\mathbf{q}})J)$ is the matrix of Coriolis and centrifugal forces, $\mathbf{g} := J^T\hat{\mathbf{g}}(\iota_Q(\mathbf{q}))$ is the vector of potential forces, $B := J^T\hat{B}(\iota_Q(\mathbf{q}))$ is the matrix of control directions, and $\boldsymbol{\lambda} := E\hat{\boldsymbol{\lambda}} \in \mathbb{R}^m$ is the vector of Lagrange multipliers.

Remark 1. In this paper, we define an explicit restriction of the system's states to a maximal integral manifold of the distribution corresponding to holonomic constraints, since uncertainties and control inputs are all originally applied in the unrestricted configuration manifold.

Pre-multiplying both sides of the set of equations representing the dynamics of the system in (6) by N^T, and substituting

$$\begin{aligned} \ddot{\mathbf{q}} &= \dot{N}(\mathbf{q},\dot{\mathbf{q}})\boldsymbol{\eta} + N(\mathbf{q})\dot{\boldsymbol{\eta}}, \\ \dot{N}(\mathbf{q},\dot{\mathbf{q}}) &= \sum_{j=1}^{n} \frac{\partial N(\mathbf{q})}{\partial \mathbf{q}_j}\dot{\mathbf{q}}_j, \end{aligned} \tag{7}$$

the set of equations on the state space of the system $\mathcal{X} \subset TQ$, which is the distribution spanned by the columns of N, is obtained as:

$$\begin{aligned} \dot{\mathbf{q}} &= N(\mathbf{q})\boldsymbol{\eta}, \\ M_r(\mathbf{q})\dot{\boldsymbol{\eta}} + C_r(\mathbf{q},\boldsymbol{\eta})\boldsymbol{\eta} + \mathbf{g_r}(\mathbf{q}) &= B_r(\mathbf{q})\boldsymbol{\tau}. \end{aligned} \tag{8}$$

Here, given $N^TA^T = 0$, the constraint forces are eliminated, and

$$\begin{aligned} M_r &:= N^TMN, \\ C_r &:= N^T(M\dot{N}(\mathbf{q}, N\boldsymbol{\eta}) + C(\mathbf{q}, N\boldsymbol{\eta})N), \\ B_r &:= N^TB, \\ \mathbf{g_r} &:= N^T\mathbf{g}, \end{aligned}$$

are respectively the reduced mass matrix, the reduced matrix of Coriolis and centrifugal forces, the reduced matrix of control directions, and the reduced vector of potential forces.

We denote a member of $\mathcal{X}$ by $\mathbf{x} = [\mathbf{q}^\mathbf{T}, \boldsymbol{\eta}^\mathbf{T}]^T$ that is a $(2n-m)$-dimensional vector of system states. The state space representation of the governing equations of motion is

$$\dot{\mathbf{x}} = \mathbf{f}(\mathbf{x}) + G(\mathbf{x})\boldsymbol{\tau}, \tag{9}$$

where

$$\mathbf{f}(\mathbf{x}) = \begin{bmatrix} N\boldsymbol{\eta} \\ -M_r^{-1}(C_r\boldsymbol{\eta} + \mathbf{g_r}) \end{bmatrix}, \quad G(\mathbf{x}) = \begin{bmatrix} \mathbb{O}_{n\times s} \\ M_r^{-1}B_r \end{bmatrix}, \tag{10}$$

and $\mathbb{O}$ denotes the matrix of zeros with proper dimensions.

III. Control Analysis

In this section, we provide a compendious control analysis of the system in (9). First, the full-state reachability and feedback linearizability are studied applying the tools presented in [32] to the category of constrained mechanical systems in (9). Then, the studies in [30], [31] are generalized to the systems

represented by (9) to investigate their input-output linearizability and the stability of their internal dynamics. Finally, we propose an observability decomposition of the internal states to improve the existing stability analysis presented in [30].

A. Reachability and Full-state Feedback Linearizability

Let us introduce the control input $\boldsymbol{\mu} \in \mathbb{R}^{n-m}$, based on

$$B_r \boldsymbol{\tau} = C_r \boldsymbol{\eta} + \mathbf{g_r} + M_r \boldsymbol{\mu}, \tag{11}$$

that partially linearizes the system in (9). Under this transformation, the resultant closed-loop system becomes

$$\begin{aligned} \dot{\mathbf{x}} &= \mathbf{f^1}(\mathbf{x}) + G^1 \boldsymbol{\mu}, \\ \mathbf{f^1}(\mathbf{x}) &= \begin{bmatrix} N\boldsymbol{\eta} \\ \mathbb{O}_{(n-m)\times 1} \end{bmatrix}, \qquad G^1 = \begin{bmatrix} \mathbb{O}_{n\times(n-m)} \\ \mathbb{I}_{(n-m)\times(n-m)} \end{bmatrix}, \end{aligned} \tag{12}$$

where $\mathbb{I}$ denotes the identity matrix with appropriate dimensions.

The control system in (12) is fully reachable if and only if for any arbitrary pair of an initial state $\mathbf{x_0}$ and a terminal state $\mathbf{x_f}$, one can find a control input $\boldsymbol{\mu}$ moving the system from $\mathbf{x_0}$ to $\mathbf{x_f}$.

Proposition 1. *The control system in (9) is fully locally reachable.*

Proof: Let $\mathcal{H}$ be a family of nonsingular involutive distributions containing the columns of G^1 and being invariant under the drift vector field $\mathbf{f^1}(\mathbf{x})$ and the columns of G^1. The family of distributions $\mathcal{H}$ has a minimal element [32]. We denote the minimal element of $\mathcal{H}$ by $\mathcal{H}_0$ that has dimension d. At each state $\mathbf{x}_0$ there is an open neighbourhood $U_0 \subset \mathbb{R}^{2n-m}$ of $\mathbf{x}_0$ on which $\mathcal{H}_0$ defines a foliation of embedded d-dimensional slices in U_0. The slice containing $\mathbf{x}_0$ is the set of all states that are reachable along trajectories of the system starting from $\mathbf{x}_0$ and staying in U_0. This slice is called the reachable set from $\mathbf{x}_0$ and it is denoted by $\mathcal{R}_{\mathbf{x}_0} \subset U_0$. Consequently, the system in (12) is fully locally reachable, if and only if $\mathcal{H}_0$ is of system's dimension, i.e., $d = 2n - m$ [32].

To construct $\mathcal{H}_0$ for the system in (12), first the distribution spanned by the columns of matrix G^1 is considered. Then, the invariance condition of $\mathcal{H}_0$ under the drift vector field $\mathbf{f^1}(\mathbf{x})$ is imposed that results in the distribution

$$\mathcal{K} := \text{im}(G^1) + \text{span}\{\mathcal{L}_{\mathbf{f^1}} G^1_j | j = 1, \cdots, n-m\}. \tag{13}$$

Here, G^1_j is the j^{th} column of G^1. The Lie derivatives in (13) are computed as:

$$\mathcal{L}_{\mathbf{f^1}} G^1_j = \frac{\partial G^1_j}{\partial \mathbf{x}} \mathbf{f^1} - \frac{\partial \mathbf{f^1}}{\partial \mathbf{x}} G^1_j. \tag{14}$$

Since G^1_j is constant based on (12), $\frac{\partial G^1_j}{\partial \mathbf{x}} = 0$. Additionally, based on (12), $\mathbf{f^1} = [(N\boldsymbol{\eta})^T \quad \mathbb{O}_{1\times(n-m)}]^T$ where N is only a function of $\mathbf{q}$; hence, we have:

$$\mathcal{L}_{\mathbf{f^1}} G^1_j = - \begin{bmatrix} \frac{\partial (N\boldsymbol{\eta})}{\partial \mathbf{q}} & N \\ \mathbb{O}_{(n-m)\times(n)} & \mathbb{O}_{(n-m)\times(n-m)} \end{bmatrix} G^1_j.$$

Accordingly, since the first n rows of G^1 are equal to zero,

$$\mathcal{K} = \text{im}(G^1) \oplus \text{im} \begin{bmatrix} -N \\ \mathbb{O}_{(n-m)\times(n-m)} \end{bmatrix}, \tag{15}$$

which is of dimension $2n - 2m$. Note that the distribution $\mathcal{K}$ defined in (15), indicates the evolution of the system in the direction of its control inputs and drift vector field. Finally, the involutivity condition is considered in construction of $\mathcal{H}_0$. Since we assumed completely nonholonomic constraints in (3), the involutivity condition of $\mathcal{H}_0$ adds m new directions when considering the Lie Brackets of vector fields in $\mathcal{K}$. Therefore, Based on dimension counting the dimension of $\mathcal{H}_0$ is equal to that of the system, and (12) is fully locally reachable. Since the system in (12) is a special case of the system in (9), its fully locally reachability can be extended to the system in (9). ■

Reachability is the necessary condition for local controllability . A fully locally reachable system is locally controllable assuming that every initial state $\mathbf{x}_0$ is in the interior of the reachable set $\mathcal{R}_{\mathbf{x}_0}$ [34].

Assumption 3. The system in (12) and hence the system in (9) is locally controllable.

Proposition 2. *The system in (9) is not full-state feedback linearizable by a smooth state feedback.*

Proof: A nonlinear control system is full-state feedback linearizable applying a smooth state feedback if and only if it is fully locally reachable and also a nested sequence of distributions defined by

$$\mathcal{F}_k := \text{span}\{\mathcal{L}^i_{\mathbf{f}} G_j | i = 0, \cdots, k-1, j = 1, \cdots, n-m\}, \tag{16}$$

for $k = 1, 2, \cdots$, are all involutive and constant dimensional [35]. G_j denotes the j^{th} column of matrix G. The distribution $\mathcal{F}_2$ is

$$\begin{aligned} \mathcal{F}_2 &= \text{im}(G) + \text{span}\{\mathcal{L}_{\mathbf{f}} G_j | j = 1, \cdots, s\} \\ &= \text{im}(G) \oplus \text{im} \begin{bmatrix} -N M_r^{-1} B_r \\ W(\mathbf{q}) \end{bmatrix}, \end{aligned} \tag{17}$$

where $W : Q \to \mathbb{R}^{(n-m)\times s}$ is a vector function determined by calculation of $\mathcal{L}_{\mathbf{f}} G_j$ using the Lie derivative equation in (14). Note that the step by step procedure of calculating $\mathcal{F}_2$ is similar to computations performed for obtaining $\mathcal{K}$ in the proof of Proposition 1 and hence it is omitted here. Based on Assumption 2 and the positive definiteness of M, the matrix $M_r^{-1} B_r$ is full-rank. Consequently, $\text{im}(G)$ covers all directions tangent to quasi velocities and $\text{im}(\begin{bmatrix} \mathbb{O}_{s\times n} & W(q)^T \end{bmatrix}^T) \subseteq \text{im}(G)$. Accordingly, if $\mathcal{F}_2$ is involutive, then $\text{im}(N)$ must be involutive. Due to the nonholonomicity of the constraints the distribution $\text{im}(N)$ is not involutive and that completes the proof. ■

B. Input-Output Linearization and Output Tracking

Let the b-dimensional vector $\mathbf{y} \in \mathbb{R}^b$ denote the output of the system in (12). We define the relationship between the states and the output of the system with the smooth function

$$\begin{aligned} \mathbf{h} &: Q \to \mathbb{R}^b \\ &\mathbf{q} \mapsto \mathbf{y} = \mathbf{h}(\mathbf{q}). \end{aligned} \tag{18}$$

The relationship between the control input and the i^{th} component of the output is obtained by ($i = 1, \cdots, b$):

$$\begin{aligned} \dot{\mathbf{y}}_i &= \mathcal{L}_{\dot{\mathbf{x}}} \mathbf{h}_i = \mathcal{L}_{\mathbf{f}^1} \mathbf{h}_i, \\ \ddot{\mathbf{y}}_i &= \mathcal{L}^2_{\dot{\mathbf{x}}} \mathbf{h}_i = \mathcal{L}^2_{\mathbf{f}^1} \mathbf{h}_i + \mathcal{L}_{G^1 \boldsymbol{\mu}} \mathcal{L}_{\mathbf{f}^1} \mathbf{h}_i. \end{aligned} \tag{19}$$

The Lie derivatives in (19) are calculated as:

$$\mathcal{L}_{\mathbf{f}^1} \mathbf{h}_i = (\frac{\partial \mathbf{h}_i}{\partial \mathbf{x}})^T \mathbf{f}^1 = (\frac{\partial \mathbf{h}_i}{\partial \mathbf{q}})^T N \boldsymbol{\eta}, \tag{20}$$

$$\begin{aligned} \mathcal{L}^2_{\mathbf{f}^1} \mathbf{h}_i = \left(\frac{\partial (\mathcal{L}_{\mathbf{f}^1} \mathbf{h}_i)}{\partial \mathbf{x}} \right)^T \mathbf{f}^1 = \boldsymbol{\eta}^T N^T \frac{\partial^2 \mathbf{h}_i}{\partial \mathbf{q}^2} N \boldsymbol{\eta} \\ + \sum_{j=1}^{n-m} \left((\frac{\partial \mathbf{h}_i}{\partial \mathbf{q}})^T \frac{\partial N_j}{\partial \mathbf{q}} N \boldsymbol{\eta} \right) \boldsymbol{\eta}_j, \end{aligned} \tag{21}$$

$$\mathcal{L}_{G^1 \boldsymbol{\mu}} \mathcal{L}_{\mathbf{f}^1} \mathbf{h}_i = (\frac{\partial \mathbf{h}_i}{\partial \mathbf{q}})^T N \boldsymbol{\mu}, \tag{22}$$

where N_j denotes the j^{th} column of the matrix N, $\boldsymbol{\eta}_j$ is the j^{th} component of the vector $\boldsymbol{\eta}$, $\frac{\partial}{\partial \mathbf{q}}$ is the Jacobian of a scalar or vector function, and $\frac{\partial^2}{\partial \mathbf{q}^2}$ denotes the Hessian of a scalar function.

Let us define the input-output decoupling matrix

$$F := \frac{\partial \mathbf{h}}{\partial \mathbf{q}} N, \tag{23}$$

and the vector function $\mathbf{w} : \mathcal{X} \to \mathbb{R}^b$, whose i^{th} component is given in (21). Then, the input-output map is described by:

$$\ddot{\mathbf{y}} = \mathbf{w} + F \boldsymbol{\mu}. \tag{24}$$

Assumption 4. Hereinafter, the dimension of the output equals to the difference between the dimension of Q and the number of completely nonholonomic constraints. i.e., $b = n - m$. Hence the decoupling matrix F is square.

Assumption 5. The decoupling matrix F is everywhere non-singular.

Remark 2. Since the output is a smooth function on Q, and based on Assumption 3 and 5, the system in (9) along with the output defined in (18) is locally input-output controllable.

Proposition 3. *Based on Assumption 4 and 5, the system in (9) along with the output defined in (18) is input-output linearizable with relative degree* 2*, applying a static state feedback.*

Proof: Based on Assumption 4 and 5, the decoupling matrix F is everywhere invertible and hence the system in (12) along with the output in (18) is input-output linearizable applying the static state feedback:

$$\boldsymbol{\mu}(\mathbf{x}, \mathbf{u}) = F^{-1}(\mathbf{q})(\mathbf{u} - \mathbf{w}), \tag{25}$$

where the vector $\mathbf{u} \in \mathbb{R}^b$ denotes the vector of control inputs in the resulting closed loop system. Under this feedback transformation, the input-output relation is in the form of a double integrator.

$$\ddot{\mathbf{y}} = \mathbf{u}. \tag{26}$$

Clearly, the control input obtained from substitution of (25) in (11) results in the same input-output linearized system in (26) for the system in (9). ■

Remark 3. All analyses presented in this paper are under the assumption that the output function $\mathbf{h}$ has been specifically selected in a manner that Assumptions 4 and 5 are satisfied.

In (26) we introduce the external dynamics of the system in (9) along with the output in (18), applying the feedback transformation in (25) and (11). Hence, the state space $\mathcal{X}$ can be partitioned into the $2b$-dimensional space of external states denoted by $\mathcal{Z}_2 \subset \mathcal{X}$ (the space of output and its velocity) and an $(n-b)$-dimensional space of the internal states, denoted by $\mathcal{Z}_1$. The external states $\mathbf{z}_2 \in \mathcal{Z}_2$ are in the following form:

$$\mathbf{z}_2 = \begin{bmatrix} \mathbf{y}^T & \dot{\mathbf{y}}^T \end{bmatrix}^T. \tag{27}$$

The components of the internal states $\mathbf{z}_1 \in \mathcal{Z}_1$ are obtained as $n-b$ arbitrary real valued functions $\mathbf{z}_{1i} : \mathcal{X} \to \mathbb{R}$ satisfying two conditions: (i) the coordinate transformation mapping $\mathfrak{T} : \mathcal{X} \to \mathcal{Z}_1 \times \mathcal{Z}_2$ that maps $\mathbf{x}$ to the vector $\mathbf{z} = [\mathbf{z}_1^T, \mathbf{z}_2^T]^T$ must be a local diffeomorphism, and (ii) the dynamics of the internal states must be independent of $\boldsymbol{\tau}$,i.e.,

$$(\frac{\partial \mathbf{z}_{1i}}{\partial \mathbf{x}})^T G = 0 \quad i = 1, \cdots, n-b. \tag{28}$$

Proposition 4. *Real-valued functions $\mathbf{z}_{1i}$ locally exist for the system in (9) with the output in (18).*

Proof: This proposition is a direct consequence of Theorem 13.1 in [16]. ■

The internal/external state decomposition (known as the normal form) for the system in (9) is expressed as:

$$\begin{aligned} \dot{\mathbf{z}}_1 &= \boldsymbol{\omega}(\mathbf{z}_1, \mathbf{z}_2), \\ \dot{\mathbf{z}}_2 &= A_c^2 \mathbf{z}_2 + B_c^2 \mathbf{u}, \end{aligned} \tag{29}$$

where the i^{th} component of $\boldsymbol{\omega}$ is

$$\boldsymbol{\omega}_i = \left(\frac{\partial \mathfrak{T}}{\partial \mathbf{x}} \mathbf{f}(\mathfrak{T}^{-1}(\mathbf{z})) \right)_i, \ i = 1 \cdots n-b, \tag{30}$$

and $A_c^2 \in \mathbb{R}^{2b \times 2b}$ and $B_c^2 \in \mathbb{R}^{2b \times b}$ are the constant matrices representing the canonical form of a chain of two integrators.

A local diffeomorphism as a state transformation can also be defined to partition the space of internal states into: (i) the a-dimensional space $\mathcal{Z}_1^o \subset \mathcal{Z}_1$ containing the observable internal states from the output in (18) for the control system in (9), and (ii) $(n-b-a)$-dimensional space $\mathcal{Z}_1^u \subset \mathcal{Z}_1$ containing the states that are unobservable from the output in (18) for both control systems in (29) and (9). Let us consider the elements $\mathbf{z}_1^o \in \mathcal{Z}_1^o$ and $\mathbf{z}_1^u \in \mathcal{Z}_u^o$. Based on this decomposition, the system in (29) can be further transformed to

$$\begin{aligned} \dot{\mathbf{z}}_1^u &= \boldsymbol{\omega}^u(\mathbf{z}_1^u, \mathbf{z}_1^o, \mathbf{z}_2), \\ \dot{\mathbf{z}}_1^o &= \boldsymbol{\omega}^o(\mathbf{z}_1^o, \mathbf{z}_2), \\ \dot{\mathbf{z}}_2 &= A_c^2 \mathbf{z}_2 + B_c^2 \mathbf{u}, \end{aligned} \tag{31}$$

where the functions $\boldsymbol{\omega}^u$ and $\boldsymbol{\omega}^o$ describe the dynamics of the observable and unobservable internal states, respectively.

Remark 4. Given the fact that the observability decomposition is dependent on the output function, this decomposition is discussed in details in Section V for a specific output function.

We denote the desired trajectories for the external states by $\mathbf{z}_{2d}(t)$, for the observable internal states by $\mathbf{z}_{1d}^o(t)$, and for the

unobservable internal states by $\mathbf{z}^u_{1d}(t)$, where $t \in \mathbb{R}^+$ refers to time.

Remark 5. Based on Assumption 3, the system in (9) is not kinematically redundant. Hence, $\mathbf{z}^o_{1d}(t)$ and $\mathbf{z}^u_{1d}(t)$ are uniquely determined based on $\mathbf{z}_{2d}(t)$ and the initial desired configuration of the system, applying the set of kinematic equations in (6).

The tracking error dynamics of the system in (31) can be formed as

$$\begin{aligned} \dot{\mathbf{z}}^u_{1e} &= \boldsymbol{\omega}^u_e(\mathbf{z}^u_{1e}, \mathbf{z}^o_{1e}, \mathbf{z}_{2e}, t), \\ \dot{\mathbf{z}}^o_{1e} &= \boldsymbol{\omega}^o_e(\mathbf{z}^o_{1e}, \mathbf{z}_{2e}, t), \\ \dot{\mathbf{z}}_{2e} &= A_c\mathbf{z}_{2e} + B_c\mathbf{v}, \end{aligned} \tag{32}$$

where $\mathbf{z}^o_{1e} := \mathbf{z}^o_1 - \mathbf{z}^o_{1d}(t)$ is the tracking error of the observable internal states, $\mathbf{z}^u_{1e} := \mathbf{z}^u_1 - \mathbf{z}^u_{1d}(t)$ is the tracking error of the unobservable internal states, $\mathbf{z}_{2e} := \mathbf{z}_2 - \mathbf{z}_{2d}$ is the tracking error of the external states and finally $\mathbf{v} := \mathbf{u} - \ddot{\mathbf{y}}_d(t)$. The functions $\boldsymbol{\omega}^u_e$ and $\boldsymbol{\omega}^o_e$ respectively describe the error dynamics of the observable and unobservable internal states, based on (31).

Remark 6. Since the elements of $\mathcal{Z}^u_1$ are not affecting the output in (18) for the control system in (9), their asymptotic stability in an output-tracking control problem is of less importance as long as they are bounded.

Problem 1 (Output-tracking Control Problem). Given a twice differentiable desired feasible trajectory $\mathbf{y_d}(\mathbf{t})$ for the output of the system, find a control law $\mathbf{v}$ that tracks $\mathbf{z_{2d}}(t)$ with an asymptotically stable tracking errors $\mathbf{z}_{2e}$ and $\mathbf{z}^o_{1e}$, and a bounded tracking error $\mathbf{z}^u_{1e}$.

The stability of the tracking error for the elements of $\mathcal{Z}^o_1$ can be investigated based on the concept of tracking-error zero dynamics . The tracking-error zero dynamics is the error dynamics of the internal states when the output error is kept identically zero applying an appropriate control input. Accordingly, the tracking-error zero dynamics of $\mathbf{z}^o_{1e}$ is

$$\dot{\mathbf{z}}^o_{1e} = \boldsymbol{\omega}^o_e(\mathbf{z}^o_{1e}, 0, t). \tag{33}$$

Assumption 6. The function $\boldsymbol{\omega}^o_e$ is locally Lipschitzian in $(\mathbf{z}^o_{1e}, \mathbf{z}_{2e})$, uniformly with respect to $t \geq 0$.

Proposition 5. *If the tracking-error zero dynamics in (33) is locally uniformly asymptotically stable, then* $\mathbf{z}^o_{1e}$ *is locally uniformly asymptotically stable, after determining* $\mathbf{v}$ *as a solution of output tracking control problem.*

Proof: Considering Assumption 6, this proposition is the direct consequence of lemma B.2.4 on page 514 in [32]. ■

Assumption 7. We assume that the tracking error $\mathbf{z}^u_{1e}$ is bounded, if the tracking errors $\mathbf{z}_{2e}$ and $\mathbf{z}^o_{1e}$ are both locally uniformly asymptotically stable and the desired trajectories are bounded.

IV. Robust Optimal Output-tracking Control

An input-output feedback linearized control system in (29) is only valid if all system's parameters are completely known and system is not subject to any disturbances. In this section, a control algorithm is proposed based on Sliding Mode Control (SMC) scheme to ensure robustness against bounded time-dependant matched uncertainties in the inertia parameters and disturbance forces.

Assumption 8. In this paper, perfect sensory data acquisition and complete knowledge of kinematic (geometric) parameters of the system is assumed.

Let us introduce a time-dependant c-dimensional vector of uncertain inertia parameters and disturbance forces $\boldsymbol{\rho}$ in a bounded neighbourhood $\mho \subset \mathbb{R}^c$, i.e., $\boldsymbol{\rho} : \mathbb{R}^+ \to \mho$. In the mechanical system described in (2), the uncertainties appear in the form of addition of uncertain terms $\Delta\hat{M} : \hat{Q} \times \mho \to \mathbb{R}^{\hat{n}\times\hat{n}}$, $\Delta\hat{C} : T\hat{Q} \times \mho \to \mathbb{R}^{\hat{n}\times\hat{n}}$, and $\Delta\hat{\mathbf{g}} : \hat{Q} \times \mho \to \mathbb{R}^{\hat{n}}$ to the mass matrix, Coriolis matrix, and the vector of potential forces, respectively. We consider disturbance forces in the following form

$$\hat{\boldsymbol{\omega}} = \sum_1^w \hat{J}_{di}\hat{\omega}_i, \tag{34}$$

where $\hat{\omega}_i$ are functions of time and $\hat{J}_{di} : \hat{Q} \to \mathbb{R}^{\hat{n}}$ are the directions of disturbance forces. Accordingly, the uncertain state space representation of the system in (9) is

$$\dot{\mathbf{x}} = \mathbf{f_u}(\mathbf{x}) + G_u(\mathbf{x})\boldsymbol{\tau}, \tag{35}$$

where

$$\mathbf{f_u}(\mathbf{x}) = \begin{bmatrix} N\boldsymbol{\eta} \\ -(M_r + \Delta M_r)^{-1}((C_r + \Delta C_r)\boldsymbol{\eta} + (\mathbf{g_r} + \boldsymbol{\Delta g_r}) - \boldsymbol{\varpi}_r) \end{bmatrix}, \tag{36}$$

$$G_u(\mathbf{x}) = \begin{bmatrix} \mathbb{O}_{n\times s} \\ (M_r + \Delta M_r)^{-1}B_r \end{bmatrix}, \tag{37}$$

and we have the terms

$$\Delta M_r := N^T J^T \Delta\hat{M} J N, \tag{38}$$

$$\begin{aligned} \Delta C_r := N^T J^T \Delta\hat{M} J\dot{N} + N^T(J^T\Delta\hat{M}\dot{J})N \\ + N^T J^T \Delta\hat{C} J N, \end{aligned} \tag{39}$$

$$\boldsymbol{\Delta g_r} := N^T J^T \Delta\hat{\mathbf{g}}, \;\; \boldsymbol{\varpi}_r := N^T J^T \hat{\boldsymbol{\omega}}. \tag{40}$$

Let us separate the nominal dynamics from the terms involving uncertainties and disturbances in (35). Applying the partially linearizing feedback in (11) and the input-output linearization feedback in (25) to the system in (35) and substituting $\boldsymbol{\eta}$ and $\dot{\boldsymbol{\eta}}$ by

$$\begin{aligned} \boldsymbol{\eta} &= F^{-1}\dot{\mathbf{y}}, \\ \dot{\boldsymbol{\eta}} &= \sum_{j=1}^b \frac{\partial F^{-1}_j}{\partial \mathbf{q}} N F^{-1}\dot{\mathbf{y}}\dot{\mathbf{y}}_j + F^{-1}\ddot{\mathbf{y}}, \end{aligned} \tag{41}$$

the resultant uncertain closed loop input-output map becomes

$$\ddot{\mathbf{y}} = \Lambda(\mathbf{q}, \boldsymbol{\rho})^{-1}(\mathbf{u} + \boldsymbol{\sigma}(\mathbf{q}, \dot{\mathbf{q}}, \boldsymbol{\rho}, \dot{\mathbf{y}})). \tag{42}$$

Here, F^{-1}_j refers to the j^{th} column of the matrix F^{-1}, $\dot{\mathbf{y}}_j$ refers to the j^{th} component of output velocity and

$$\Lambda := \mathbb{I}_{b\times b} + F M_r^{-1} \Delta M_r F^{-1}, \tag{43}$$

$$\boldsymbol{\sigma} := FM_r^{-1}(-\Delta M_r \sum_{j=1}^{b} \frac{\partial F_j^{-1}}{\partial q} NF^{-1}\dot{\mathbf{y}}\dot{\mathbf{y}}_j - \Delta C_r F^{-1}\dot{\mathbf{y}} - \Delta \mathbf{g_r} + \boldsymbol{\varpi}_r). \quad (44)$$

Assumption 9. We assume the bound $\left\|FM_r^{-1}\Delta M_r F^{-1}\right\| < \epsilon_1 < \frac{1}{1+\sqrt{2}}$, where the operator $\|\|$ denotes the square Frobenius norm of a matrix and ϵ_1 is a constant real number.

Assumption 10. In many applications of the developed theory, the dimension of the output $b = n-m = 2$. Examples include different types of autonomous rovers, under water or aerial vehicles moving in a plane. Therefore, we assume $b = 2$ in the rest of the paper. With some extra work, the analysis presented in this paper may be extended to higher dimensional outputs.

Consequently based on Assumption 9 and 10, the determinant of matrix Λ is always strictly positive. Hence, this matrix is always invertible and its diagonal elements are strictly positive. The state-space representation of the error-dynamics of the uncertain mapping in (42) becomes:

$$\ddot{\mathbf{e}} = \Lambda(\mathbf{q},\boldsymbol{\rho})^{-1}(\mathbf{v} + \boldsymbol{\sigma}_e(\mathbf{q},\boldsymbol{\rho},\dot{\mathbf{e}},t)), \quad (45)$$

where $\mathbf{e} = \mathbf{y} - \mathbf{y}_d$, and $\boldsymbol{\sigma}_e = \boldsymbol{\sigma} + (\mathbb{I} - \Lambda)\ddot{\mathbf{y}}_d$.

Assumption 11. $\|\boldsymbol{\sigma}_e\| < \epsilon_2$, where ϵ_2 is a constant real number.

Sliding mode control as a variable structure control method can be applied to the system in (45) to stabilize the tracking error of the output, which guarantees robustness against bounded uncertainties. The design of SMC is performed in two steps: (i) designing the sliding manifold on which error becomes asymptotically stable towards the origin, (ii) designing a switching control law pushing a system outside of the sliding manifold towards it. Accordingly, the control law designed based on SMC consists of an equivalent control input denoted by the 2-dimensional vector $\mathbf{v}_{eq}$ associated with the motion on the sliding manifold, and a switching control law denoted by the 2-dimensional vector $\mathbf{v}_s$, i.e.,

$$\mathbf{v} = \mathbf{v}_{eq} + \mathbf{v}_s. \quad (46)$$

A. Optimal Sliding Manifold Design

The sliding manifold determines the convergence behaviour of the output error to zero, when the system operates in nominal conditions (with no uncertainties and disturbances). Considering the nominal linearized input-output map in (26) along with an integral action to eliminate steady state error and improve robustness, the state space representation of the error dynamics becomes :

$$\dot{\mathbf{y}}_e = A_c^3\mathbf{y}_e + B_c^3\mathbf{v}_{eq}, \quad (47)$$

where

$$\mathbf{y}_e := \left[\left(\int_0^t \mathbf{e}^T(\tau)d\tau\right)\ \mathbf{e}^T\ \dot{\mathbf{e}}^T\right]^T \in \mathbb{R}^6,$$

and $A_c^3 \in \mathbb{R}^{6\times6}$ and $B_c^3 \in \mathbb{R}^{6\times2}$ are the constant matrices representing the canonical form of a chain of three integrators.

Problem 2 (LQR Control Problem). In system (47) find the control input $\mathbf{v}_{eq}(t)$ to asymptotically stabilize the origin for $\mathbf{y}_e$, while reaching the origin in a pre-specified finite time t_f and minimizing the following performance measure functional,

$$\Pi(\mathbf{v}_{eq}(t),\mathbf{e}(t)) = \frac{1}{2}\int_0^{t_f}\left(\mathbf{v}_{eq}^T K_v \mathbf{v}_{eq} + \mathbf{e}^T K_e \mathbf{e}\right)dt, \quad (48)$$

where K_v and K_e are both 2×2 positive definite diagonal weighting matrices.

The solution can be found based on the variational principle. We first form the Hamiltonian function $\mathscr{H}$ as :

$$\mathscr{H}(\mathbf{v}_{eq},\mathbf{y}_e,\mathbf{p}) = \mathbf{v}_{eq}^T K_v \mathbf{v}_{eq} + \mathbf{e}^T K_e \mathbf{e} + \mathbf{p}^T\dot{\mathbf{y}}_e(\mathbf{v}_{eq},\mathbf{y}_e), \quad (49)$$

where the 6-dimensional vector $\mathbf{p}$ is a vector of Lagrange multipliers, i.e., co-states, and the functionality of $\dot{\mathbf{y}}_\mathbf{e}$ is in (47). The necessary conditions for the optimal trajectory and the optimal control input beside the constraint coming from the error dynamics in (47) are [36]:

$$\dot{\mathbf{p}}^* = -\frac{\partial\mathscr{H}}{\partial\mathbf{y}_e}(\mathbf{y}_e^*,\mathbf{v}_{eq}^*,\mathbf{p}^*), \quad (50)$$

$$0 = \frac{\partial\mathscr{H}}{\partial\mathbf{v}_{eq}}(\mathbf{y}_e^*,\mathbf{v}_{eq}^*,\mathbf{p}^*) \Rightarrow \mathbf{v}_{eq}^* = -K_v^{-1}\left[\mathbb{O}_{2\times4}\quad \mathbb{I}_{2\times2}\right]\mathbf{p}^*, \quad (51)$$

where the superscript asterisk refers to the optimal curves. Substituting $\mathbf{v}_{\mathbf{eq}}^*$ in (47) and (50), the 12 number of linear first order ordinary differential equations known as the reduced state co-state equations become:

$$\dot{\mathbf{x}}_{ep}^* = A_L\mathbf{x}_{ep}^*, \quad (52)$$

where the 12-dimensional vector $\mathbf{x}_{ep}^* = [(\mathbf{y}_e^*)^T,(\mathbf{p}^*)^T]^T$ and $A_L \in \mathbb{R}^{12\times12}$ is a constant matrix (see Appendix I). The solution of this equation is

$$\mathbf{x}_{ep}^* = B_L(t)\mathbf{x}_{ep}^*(t_0), \quad (53)$$

where $B_L = \exp(A_L t)$ is the state transition matrix.

Let $B_{Lf} = B_L(t_f)$, which can be partitioned as

$$B_{Lf} = \begin{bmatrix} B_{Lf1,1} & B_{Lf1,2} \\ B_{Lf2,1} & B_{Lf2,2,} \end{bmatrix}, \quad (54)$$

where $B_{Lfi,j} \in \mathbb{R}^{6\times6}$ $(i,j = 1,2)$. Considering the split boundary value conditions $\mathbf{y}_\mathbf{e}^*(t_f) = 0$ and $\mathbf{y}_\mathbf{e}^*(0) = \mathbf{y_e}$, the optimal control input $\mathbf{v}_{\mathbf{eq}}^*$ is obtained in the form of a PID controller. We set the equivalent control input $\mathbf{v_{eq}}$ as

$$\mathbf{v}_{eq} = \mathbf{v}_{eq}^* = -\begin{bmatrix} K_I^* & K_p^* & K_d^* \end{bmatrix}\mathbf{y}_e, \quad (55)$$

where the matrix of optimal gains is:

$$\begin{bmatrix} K_I^* & K_p^* & K_d^* \end{bmatrix} = -K_v^{-1}\left[\mathbb{O}_{2\times4}\quad \mathbb{I}_{2\times2}\right]B_{Lf12}^{-1}B_{Lf11}. \quad (56)$$

The matrix B_{Lf12} based on the structure of matrix A_L is invertible (see Appendix I). The obtained control law in (55) results in the convergence of the error on the following manifold

$$\ddot{\mathbf{e}} + K_d^*\dot{\mathbf{e}} + K_p^*\mathbf{e} + K_I^*\int_0^t \mathbf{e}(\tau)d\tau = 0. \quad (57)$$

Integrating this manifold, the following 2-dimensional relative degree one sliding manifold $\mathbf{s}$ is designed:

$$\mathbf{s} = \dot{\mathbf{e}} + K_d^* \mathbf{e} + K_p^* \int_0^t \mathbf{e}(\tau) d\tau + K_I^* \int_0^t \left(\int_0^\tau \mathbf{e}(\tau_1) d\tau_1 \right) d\tau = 0. \tag{58}$$

B. Switching Control Law

After designing an optimal sliding manifold, the switching control law $\mathbf{v_s}$ is obtained based on the uncertain error dynamics in (45), such that the sliding manifold $\mathbf{s} = 0$ is attractive in finite time. Let us define the function $\alpha(\mathbf{y_e})$ and the constant k_0 as

$$\alpha(\mathbf{y}_e) := \frac{(\sqrt{2}+\epsilon_1)(\|\mathbf{v}_{eq}\|+\epsilon_2)+\|\mathbf{v}_{eq}\|}{1-\epsilon_1}, \tag{59}$$

$$k_0 := \frac{\epsilon_1}{1-\epsilon_1}. \tag{60}$$

Theorem 1. *For any function β satisfying the condition*

$$\beta(\mathbf{y}_e) \geq \frac{\alpha}{1-\sqrt{2}k_0} + \beta_0, \tag{61}$$

where β_0 is a strictly positive arbitrary constant, the switching control law,

$$\mathbf{v}_{si} = -\beta sgn(\mathbf{s}_i) \tag{62}$$

makes the system in (42) asymptotically stable towards the optimal sliding manifold in (58) as long as $\left\|FM_r^{-1}\Delta M_r F^{-1}\right\| < \epsilon_1 < \frac{1}{1+\sqrt{2}}$ and $\|\boldsymbol{\sigma}_e\| < \epsilon_2$.

Proof: Prior to providing the stability proof of the proposed switching control law, let us remind some important properties of the matrix Λ. Based on Assumptions 9, 10, and 11, we have:

(i) Due to triangle inequality, $\sqrt{2}-\epsilon_1 < \|\Lambda\| < \sqrt{2}+\epsilon_1$.

(ii) Decomposing Λ into matrices of its diagonal elements Λ_d and its off-diagonal elements Λ_o, i.e., $\Lambda = \Lambda_d + \Lambda_o$, it can be deduced that $\|\Lambda_o\| < \epsilon_1$, and the diagonal elements of Λ_d are strictly positive.

(iii) The determinant of Λ is strictly positive.

(iv) Since Λ is two by two, $\left\|\Lambda^{-1}\right\| = \frac{\|\Lambda\|}{\det(\Lambda)}$.

(v) The matrix Λ^{-1} can be also decomposed into the matrices of its diagonal elements Λ_d^{-1} and its off-diagonal elements Λ_o^{-1}, i.e., $\Lambda^{-1} = \Lambda_d^{-1} + \Lambda_o^{-1}$. Since Λ is two by two, it can be deduced that $\left\|\Lambda_o^{-1}\right\| = \frac{\|\Lambda_o\|}{\det(\Lambda)}$ and $\left\|\Lambda_d^{-1}\right\| = \frac{\|\Lambda_d\|}{\det(\Lambda)}$.

For stability proof, we consider the following positive definite function as a Lyapunov candidate

$$V(\mathbf{s}) = \frac{1}{2}\mathbf{s}^T\mathbf{s}. \tag{63}$$

The time derivative of V is

$$\dot{V} = \mathbf{s}^T\dot{\mathbf{s}} = \mathbf{s}^T[\Lambda^{-1}(\mathbf{v}_s + \mathbf{v}_{eq} + \boldsymbol{\sigma}_e) + \mathbf{v}_{eq}], \tag{64}$$

using the definition of the sliding surface in (58) and $\mathbf{v}_{eq}$ in (55), and the uncertain error dynamics in (45). We write $\dot{V} = \dot{V}_1 + \dot{V}_2$, where $\dot{V}_i = \mathbf{s}_i\dot{\mathbf{s}}_i$, for $i = 1, 2$. Decomposing the matrix Λ^{-1} into the matrices of its diagonal elements Λ_d^{-1} and its off-diagonal elements Λ_o^{-1}, (64) becomes:

$$\dot{V} = \mathbf{s}^T\Lambda_d^{-1}\mathbf{v}_s + \mathbf{s}^T\Lambda_o^{-1}\mathbf{v}_s + \mathbf{s}^T[\Lambda^{-1}(\mathbf{v}_{eq}+\boldsymbol{\sigma}_e)+\mathbf{v}_{eq}]. \tag{65}$$

Hence,

$$\dot{V}_i \leq \mathbf{s}_i\Lambda_{di}^{-1}\mathbf{v}_{si} + |\mathbf{s}_i|(\left\|\Lambda_o^{-1}\right\|\|\mathbf{v}_s\| + \left\|\Lambda^{-1}\right\|(\|\mathbf{v}_{eq}\| + \|\boldsymbol{\sigma}_e\|) + \|\mathbf{v}_{eq}\|), \tag{66}$$

where Λ_{di}^{-1} refers to the i^{th} diagonal element of matrix Λ_d^{-1}, and $\mathbf{s}_i$ denotes the i^{th} component of vector $\mathbf{s}$. Since Λ_{di}^{-1} is a positive number,

$$\frac{\dot{V}_i}{\Lambda_{di}^{-1}} \leq \mathbf{s}_i\mathbf{v}_{si} + |\mathbf{s}_i|\frac{\left\|\Lambda_o^{-1}\right\|\|\mathbf{v}_s\|}{\Lambda_{di}^{-1}} + |\mathbf{s}_i|\frac{\left\|\Lambda^{-1}\right\|(\|\mathbf{v}_{eq}\| + \|\boldsymbol{\sigma}_e\|) + \|\mathbf{v}_{eq}\|)}{\Lambda_{di}^{-1}}. \tag{67}$$

Considering the norm inequality for a diagonal element of Λ, i.e., $1-\epsilon_1 < \Lambda_{di}$, and based on property (v) for the matrix Λ, an upper bound for the right hand side of (67) is obtained by substituting a lower bound of the denominators.

$$\begin{aligned}\frac{\dot{V}_i}{\Lambda_{di}^{-1}} &\leq \mathbf{s}_i\mathbf{v}_{si} + |\mathbf{s}_i|\frac{\det(\Lambda)\left\|\Lambda_o^{-1}\right\|\|\mathbf{v}_s\|}{1-\epsilon_1} \\ &\quad + |\mathbf{s}_i|\frac{\det(\Lambda)\left\|\Lambda^{-1}\right\|(\|\mathbf{v}_{eq}\| + \|\boldsymbol{\sigma}_e\|) + \|\mathbf{v}_{eq}\|)}{1-\epsilon_1} \\ &= \mathbf{s}_i\mathbf{v}_{si} + |\mathbf{s}_i|\frac{\|\Lambda_o\|\|\mathbf{v}_s\|}{1-\epsilon_1} \\ &\quad + |\mathbf{s}_i|\frac{\|\Lambda\|(\|\mathbf{v}_{eq}\| + \|\boldsymbol{\sigma}_e\|) + \|\mathbf{v}_{eq}\|)}{1-\epsilon_1}. \end{aligned} \tag{68}$$

Based on properties (i) and (ii) for the matrix Λ and Assumption 11, an upper bound for the right hand side of (68) is obtained by substituting the upper bounds of the nominators. According to (59) and (60) we have

$$\begin{aligned}\frac{\dot{V}_i}{\Lambda_{di}^{-1}} &\leq \mathbf{s}_i\mathbf{v}_{si} + |\mathbf{s}_i|\frac{\epsilon_1\|\mathbf{v}_s\|}{1-\epsilon_1} + |\mathbf{s}_i|\frac{(\sqrt{2}+\epsilon_1)(\|\mathbf{v}_{eq}\|+\epsilon_2)+\|\mathbf{v}_{eq}\|)}{1-\epsilon_1} \\ &= \mathbf{s}_i\mathbf{v}_{si} + |\mathbf{s}_i|(\alpha + k_0\|\mathbf{v}_s\|). \end{aligned} \tag{69}$$

Substituting $\mathbf{v}_{si}$ from (62) and considering the fact that $\|\mathbf{v_s}\| \leq \sqrt{2}\beta$, we obtain

$$\begin{aligned}\frac{\dot{V}_i}{\Lambda_{di}^{-1}} &\leq -\beta\mathbf{s}_i sgn(\mathbf{s}_i) + |\mathbf{s}_i|(\alpha + \sqrt{2}k_0\beta) \\ &= |\mathbf{s}_i|(\alpha - \beta(1-\sqrt{2}k_0)). \end{aligned} \tag{70}$$

Since based on Assumption 9, $1-\sqrt{2}k_0 > 0$, it can be deduced from (61) that $-\beta(1-\sqrt{2}k_0) \leq -\alpha - \beta_0(1-\sqrt{2}k_0)$. Hence,

$$\frac{\dot{V}_i}{\Lambda_{di,i}^{-1}} \leq -|\mathbf{s}_i|(\beta_0(1-\sqrt{2}k_0)) < 0. \tag{71}$$

Since $\dot{V} = \dot{V}_1 + \dot{V}_2$, the inequality in (71) guarantees that $\dot{V}$ is negative definite under the assumptions of the theorem and

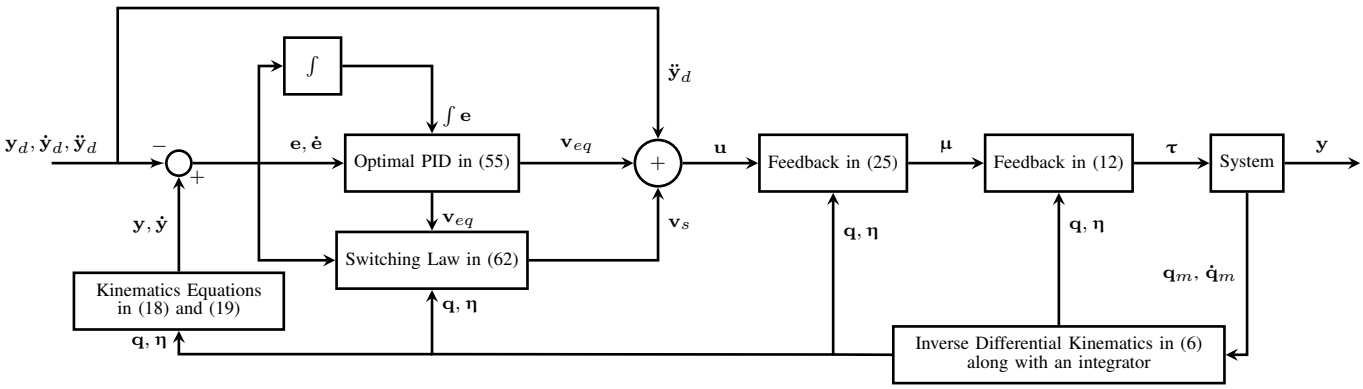

Fig. 1: Optimal output-tracking sliding mode control block diagram

the closed-loop system is stable towards the sliding manifold $\mathbf{s} = 0$. ■

To alleviate the chattering effects, the sign function in the switching control law (62) can be approximated by a high-slope continuous saturation function

$$\mathbf{v}_{si} = -\beta(\mathbf{y}_e)\text{sat}(\frac{\mathbf{s}_i}{\kappa}), \tag{72}$$

where for a constant $0 < \kappa \ll 1$

$$\text{sat}(\frac{\mathbf{s}_i}{\kappa}) := \begin{cases} -1 & \mathbf{s}_i \leq -\kappa, \\ \frac{\mathbf{s}_i}{\kappa} & -\kappa < \mathbf{s}_i < \kappa, \\ +1 & \mathbf{s}_i \geq \kappa. \end{cases}$$

Based on the switching control law in (72), the two components of the Lyapunov function V, i.e., V_1 and V_2, satisfy the following inequality instead of (69):

$$\frac{\dot{V}_i}{\Lambda_{di}^{-1}} \leq -\beta \mathbf{s}_i \text{sat}(\frac{\mathbf{s}_i}{\kappa}) + |\mathbf{s}_i|(\alpha + k_0\|\mathbf{v}_s\|). \tag{73}$$

Clearly in the region where $|\mathbf{s}_i| \geq \kappa$ (for $i = 1, 2$), the inequality (71) still holds; and hence the system in (42) reaches the boundary layer $|\mathbf{s}_i| \leq \kappa$ (for $i = 1, 2$) around the optimal sliding manifold (58) in finite time and remains inside thereafter.

Remark 7. Inside of the boundary layer $|\mathbf{s}_i| \leq \kappa$ (for $i = 1, 2$) around the optimal sliding manifold, the vector $\mathbf{y}_e$ is bounded and reaches a positively invariant set in finite time. This leads to tracking with a guaranteed precision which can be arbitrarily adjusted by choosing κ [16], [33].

The block diagram of the proposed control strategy is depicted in Fig. 1, where the vectors $\mathbf{q}_m$ and $\dot{\mathbf{q}}_m$ are the set of measurable generalized coordinates and velocities. The states and the outputs of the system that are not measurable can be computed using the inverse differential kinematics relationship in (6) based on the nonholonomic constraints and the kinematics equations in (18) and (19), respectively.

Remark 8. If $s > n - m$, i.e., if the system contains redundant control directions, the matrix B_r in (11) is not a square invertible matrix. Accordingly, specifying the vector of control inputs $\boldsymbol{\mu}$ to accomplish a control task does not result in a unique solution for the control inputs $\boldsymbol{\tau}$ in (8). In this paper, the right pseudo-inverse algorithm is employed to find a solution for $\boldsymbol{\tau}$ that minimizes the quadratic norm of the control actions.

Remark 9. If the system starts its motion with an initial error, it might be far from the optimal sliding manifold in (58). This can result in producing large amounts of control actions by the proposed switching control law at the beginning of the motion. This drawback can be rectified by properly setting initial values for the integral or double integral terms in (58) in order for the system to start its motion on the sliding manifold.

V. Implementation on a Six-wheel Type $(1, 1)$ Autonomous Lunar Rover

In this section, the developed theory is implemented on a Lunar six-wheel type $(1, 1)$ autonomous rover. Type $(1, 1)$ autonomous rovers is referring to the category of such systems whose motion in only one direction (forward/backward) can be directly controlled and their orientation is indirectly controlled during the forward/backward motion through a single steering command [37].

Remark 10. In type $(1, 1)$ autonomous rovers, system may contain more than one steering degree-of-freedom, but to ensure mobility of the system axes of rotations of all steerable wheels must intersect at the center of turning (Ackerman Condition). See Fig. 2. This results in holonomic constraints between steering degrees of freedom and hence system indirectly rotates by a single steering command.

The system under study can be modelled as the composition of a main body which is the most massive part of the rover and six driven wheels located on three parallel axes and connected to the main body by ideal joints. Wheels located on centre and rear axes can only have axial rotation while the front wheels are allowed to have both steering and axial rotation relative to the main body. To each part, a body-fixed coordinate frame is assigned. For the main body, the origin of the coordinate frame is located at the middle of the center wheels' axis, its x-axis is aligned with the rover's forward direction of motion and its y-axis is in the lateral direction pointing towards the port side (xy-frame). For the wheels, the assigned body coordinate frames are located at the centre of the wheels and their axes are parallel to those of main body frame when axial rotation and steering angles are all equal to zero. The schematic of the

system is depicted in Fig. 2, where x_0y_0-frame is the inertial coordinate frame, the vector $[x_{cm}\ y_{cm}]^T$ denotes the position of the main body's centre of mass in xy-frame, $2c$ is the lateral distance between the wheels, and L and L_0 are respectively the longitudinal distances between the front and rear wheels from the origin of xy-frame. Further, the radius of the wheels is denoted by R_w. Assuming that the system only has planar

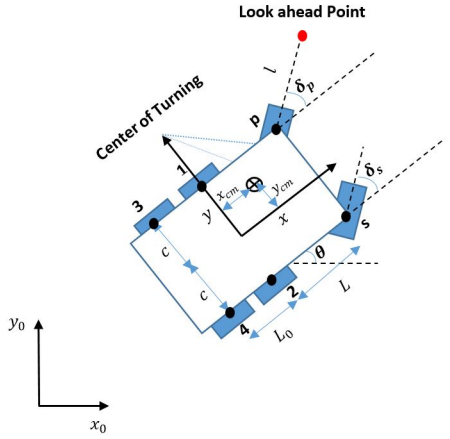

Fig. 2: schematic of the system

motion, the configuration manifold of the system $\hat{Q} = \mathbb{R}^2 \times \mathbb{T}^9$ (Cartesian product of $\mathbb{R}^2$ and 9-torus) is 11 dimensional, i.e., $\hat{n} = 11$, and the generalized coordinates of the system are

$$\hat{\mathbf{q}} = \begin{bmatrix} x_b\ y_b\ \theta\ \psi_s\ \delta_s\ \psi_1\ \psi_2\ \psi_3\ \psi_4\ \psi_p\ \delta_p \end{bmatrix}^T \in \hat{Q}. \tag{74}$$

Here, $[x_b\ y_b\ \theta]^T \in \mathbb{R}^2 \times \mathbb{T}^1$ is the position and orientation of xy-frame from x_0y_0-frame and expressed in the inertial frame, $\psi_s, \psi_p \in \mathbb{T}^1$ are respectively the rotation of the starboard and port front wheels, $\delta_s, \delta_p \in \mathbb{T}^1$ are the steering angle of the starboard and port front wheels, respectively, and $\psi_1, \psi_2, \psi_3, \psi_4, \in \mathbb{T}^1$ refer to the axial rotations of port center wheel, starboard center wheel, port rear wheel, and starboard rear wheel, respectively.

The imposed constraints on the system are (i) a constraint between steering angles of the front wheels due to the Ackerman condition, and (ii) the no longitudinal and lateral slip condition at all wheels, except rear wheels. Considering the rover's mobility, the no-lateral velocity constraint at the rear wheels is relaxed in this paper, and they are assumed to skid-steer.

Accordingly, the number of everywhere linearly independent constraints is $r = 9$ and the constraint matrix $\hat{A}$ is formed as in (75). The first row of $\hat{A}$ captures the constraint between the steering degrees of freedom, where

$$\delta_s = f_A(\delta_p) = \tan^{-1}\left(\frac{\tan(\delta_p)}{1 + \frac{2c\tan(\delta_p)}{L}}\right). \tag{76}$$

The second and third rows of $\hat{A}$ refer to the no-lateral velocity constraint at the wheel-ground contact point of the port front wheel and the center wheels, respectively. The remaining rows correspond to the no-longitudinal velocity constraint at the wheel-ground contact point of all six wheels.

Remark 11. Since the center wheels are always parallel, their corresponding no-lateral velocity constraints are linearly dependant. Hence, to include both constraints only one equation is considered when forming $\hat{A}$. Further, since the steering angles are assumed to satisfy the Ackerman condition, the no-lateral velocity constraint at the starboard front wheel is linearly dependant on the second and third rows of $\hat{A}$; and hence it is excluded, when forming $\hat{A}$.

Based on the Lagrange d'Alembert principle, the equations of motion of the rover are derived. The matrices $\hat{M}(\theta)$ and $\hat{C}(\theta, \dot{\hat{\mathbf{q}}})$ in (2) are obtained and presented in Appendix II. Assuming that only planar motion is allowed, the vector $\hat{\mathbf{g}} \equiv 0$. The vector of control inputs $\boldsymbol{\tau}$ consists of the torques applied to all wheels collocated to their axial motion along with the steering torques applied to the front wheels, i.e., $\dim(\boldsymbol{\tau}) = s = 8$ and the matrix of control directions $\hat{B}$ is

$$\hat{B} = \begin{bmatrix} \mathbb{O}_{8\times 3} & \mathbb{I}_{8\times 8} \end{bmatrix}^T. \tag{77}$$

Based on the imposed constraints, one possible everywhere nonsingular choice of matrix $\hat{N}$ is:

$$\hat{N} = \begin{bmatrix} \frac{R_w}{L}\cos(\theta)(L\cos(\delta_p) + c\sin(\delta_p)) & 0 \\ \frac{R_w}{L}\sin(\theta)(L\cos(\delta_p) + c\sin(\delta_p)) & 0 \\ \frac{R_w}{L}\sin(\delta_p) & 0 \\ \hat{N}_{4,1} & 0 \\ 0 & \hat{N}_{5,2} \\ \cos(\delta_p) & 0 \\ \frac{2c}{L}\sin(\delta_p) + \cos(\delta_p) & 0 \\ \cos(\delta_p) & 0 \\ \frac{2c}{L}\sin(\delta_p) + \cos(\delta_p) & 0 \\ 1 & 0 \\ 0 & 1 \end{bmatrix}, \tag{78}$$

where

$$\hat{N}_{4,1} = \sin(\delta_p)\left(\frac{2c}{L}\cos(\delta_s) + \sin(\delta_s)\right) + \cos(\delta_p)\cos(\delta_s),$$

$$\hat{N}_{5,2} = \frac{L^2}{2c^2 + L^2 - 2c^2\cos(2\delta_p) + 2cL\sin(2\delta_p)}.$$

To investigate the nonholonomicity of the constraints in (75), the involutive closure of the distribution $\mathcal{D} = \mathrm{im}(\hat{N})$ needs to be calculated. Let us form the distribution $\mathcal{D}_1 = \mathrm{span}\{\hat{N}_1, \hat{N}_2, \mathbf{n}_1\}$ where $\hat{N}_1$ and $\hat{N}_2$ respectively are the first and the second column of $\hat{N}$ and $\mathbf{n}_1 = \mathcal{L}_{\hat{N}_1}\hat{N}_2$. The Lie derivative $\mathcal{L}_{\hat{N}_1}\hat{N}_2$ is calculated based on (14) and it is verified to be linearly independent of $\hat{N}_1$ and $\hat{N}_2$ using Wolfram Mathematica Symbolic Software. Note that the final form of the calculated Lie derivatives are excluded due to space considerations. Similarly, in the next step, the distribution $\mathcal{D}_2 = \mathrm{span}\{\hat{N}_1, \hat{N}_2, \mathbf{n}_1, \mathbf{n}_2, \mathbf{n}_3\}$ is formed where $\mathbf{n}_2 = \mathcal{L}_{\hat{N}_1}\mathbf{n}_1$ and $\mathbf{n}_3 = \mathcal{L}_{\hat{N}_2}\mathbf{n}_1$ which is of dimension 5. Finally, following the same pattern, the 7-dimensional distribution $\mathcal{D}_3 = \mathrm{span}\{\hat{N}_1, \hat{N}_2, \mathbf{n}_1, \mathbf{n}_2, \mathbf{n}_3, \mathbf{n}_4, \mathbf{n}_5\}$ is calculated where

$\mathbf{n}_4 = \mathcal{L}_{\hat{N}_1}\mathbf{n}_2$ and $\mathbf{n}_5 = \mathcal{L}_{\hat{N}_2}\mathbf{n}_2$. Calculating the Lie derivatives between the basis elements of $\mathcal{D}_3$, and investigating their linear dependency to the basis elements of $\mathcal{D}_3$ in Mathematica, it is deduced that $\mathcal{D}_3$ is the involutive closure of $\mathcal{D}$. According to the dimension of $\mathcal{D}_3$, the system experiences $9-(11-7)=5$ completely nonholonomic constraints. In addition to the Ackerman condition, which is the holonomic constraint reflected in the first row of $\hat{A}$, system experiences three other holonomic constraints:

(i) Subtracting the constraint equation associated with the seventh row of $\hat{A}$ from that associated with its sixth row leads to a holonomic constraint between the rotation of the main body and axial rotations of the center wheels:

$$-2c\dot{\theta}-R_w(\dot{\psi}_1-\dot{\psi}_2)=0 \Rightarrow \theta-\frac{R_w}{2c}(\psi_2-\psi_1)=0. \quad (79)$$

(ii) Similarly, repeating the same procedure for the last two rows of $\hat{A}$, we obtain:

$$-2c\dot{\theta}-R_w(\dot{\psi}_4-\dot{\psi}_3)=0 \Rightarrow \theta-\frac{R_w}{2c}(\psi_4-\psi_3)=0. \quad (80)$$

Accordingly by equating (79) and (80), the following equivalent holonomic constraint is obtained.

$$(\psi_2-\psi_1)-(\psi_4-\psi_3)=0. \quad (81)$$

(iii) Finally, subtracting the summation of the constraint equations corresponding to the sixth and seventh rows of $\hat{A}$ from the summation of the constraint equations corresponding to its last two rows, the following holonomic constraint is formed.

$$(\dot{\psi}_2+\dot{\psi}_1)-(\dot{\psi}_4+\dot{\psi}_3)=0 \Rightarrow (\psi_2+\psi_1)-(\psi_4+\psi_3)=0 \quad (82)$$

Assumption 12. In this paper, it is assumed that based on the assignment of body coordinate frames, the integration constant after integrating the holonomic constraint equations are all equal to zero.

Combining (79)-(82), we derive the following set of holonomic constraint equations to be imposed on the system.

$$\theta-\frac{R_w}{2c}(\psi_2-\psi_1)=0, \quad \psi_1-\psi_3=0, \quad \psi_2-\psi_4=0. \quad (83)$$

According to all holonomic constraints, we form the 7-dimensional restricted configuration manifold $Q=\mathbb{R}^2\times\mathbb{T}^5$ whose elements are denoted by $\mathbf{q}=[x_b\ y_b\ \psi_s\ \psi_1\ \psi_2\ \psi_p\ \delta_p]^T$ and we have the inclusion map

$$\hat{\mathbf{q}}=\iota_Q(\mathbf{q})=[x_b \quad y_b \quad \tfrac{R_w}{2c}(\psi_2-\psi_1) \quad \psi_s \quad f_A(\delta_p) \quad \psi_1 \quad \psi_2 \quad \psi_1 \quad \psi_2 \quad \psi_p \quad \delta_p]^T. \quad (84)$$

Therefore, the nonzero elements of the Jocabian of this inclusion map J are

$$\begin{aligned} J_{1,1}&=J_{2,2}=J_{4,3}=J_{6,4}=J_{7,5}\\ &=J_{8,4}=J_{9,5}=J_{10,6}=J_{11,7}=1,\\ J_{3,4}&=-J_{3,5}=\frac{-R_w}{2c}, \quad J_{5,7}=\frac{df_A}{d\delta_p}(\delta_p). \end{aligned} \quad (85)$$

The constraint matrix A associated with the remaining linearly independent nonholonomic constraints is obtained based on (4), where the matrix $E=\begin{bmatrix}\mathbb{O}_{5\times1} & \mathbb{I}_{5\times5} & \mathbb{O}_{5\times3}\end{bmatrix}$. We choose the directly measurable states of the rotational velocity and steering velocity of the port front wheel as the 2-dimensional quasi-velocity vector, i.e., $\boldsymbol{\eta}=\begin{bmatrix}\dot{\psi}_p & \dot{\delta}_p\end{bmatrix}^T$. Hence, the matrix N is identified as

$$N=\begin{bmatrix} \frac{R_w}{L}\cos(\theta)(L\cos(\delta_p)+c\sin(\delta_p)) & 0\\ \frac{R_w}{L}\sin(\theta)(L\cos(\delta_p)+c\sin(\delta_p)) & 0\\ \hat{N}_{4,1} & 0\\ \cos(\delta_p) & 0\\ \frac{2c}{L}\sin(\delta_p)+\cos(\delta_p) & 0\\ 1 & 0\\ 0 & 1 \end{bmatrix}. \quad (86)$$

The reduced state space representation in (9) for the autonomous Lunar rover can now be formulated based on the determined matrices $N, J, \hat{B}, \hat{M}$, and $\hat{C}$ (see Appendix II), and the definition of $\boldsymbol{\eta}$ and the map ι_Q. Note that the vector of system states is $\mathbf{x}=[\mathbf{q}^{\mathbf{T}},\boldsymbol{\eta}^{\boldsymbol{T}}]^T\in\mathcal{X}$.

The output functions for various types of rovers that make the system in (9) input-output linearizable by applying static state feedback is presented in [30]. The type $(1,1)$ autonomous rover systems are input-output linearizable by applying static state feedback, if the inertial location of a virtual reference point in front of the steerable port front wheel (look-ahead point) is defined as the output (see Fig.2). This output function and its corresponding decoupling matrix F are respectively

$$\mathbf{y}(\mathbf{q})=\begin{bmatrix}x_b+L\cos(\theta)-c\sin(\theta)+l\cos(\delta_p+\theta)\\ y_b+L\sin(\theta)+c\cos(\theta)+l\sin(\delta_p+\theta)\end{bmatrix}, \quad (87)$$

$$\hat{A}(\hat{q})=\begin{bmatrix} 0 & 0 & 0 & 0 & 1 & 0 & 0 & 0 & 0 & 0 & -\frac{df_A}{d\delta_p}\\ -\sin(\delta_p+\theta) & \cos(\delta_p+\theta) & L\cos(\delta_p)+c\sin(\delta_p) & 0 & 0 & 0 & 0 & 0 & 0 & 0 & 0\\ -\sin(\theta) & \cos(\theta) & 0 & 0 & 0 & 0 & 0 & 0 & 0 & 0 & 0\\ \cos(\delta_p+\theta) & \sin(\delta_p+\theta) & L\sin(\delta_p)-c\cos(\delta_p) & 0 & 0 & 0 & 0 & 0 & 0 & -R_w & 0\\ \cos(\delta_s+\theta) & \sin(\delta_s+\theta) & L\sin(\delta_s)+c\cos(\delta_s) & -R_w & 0 & 0 & 0 & 0 & 0 & 0 & 0\\ \cos(\theta) & \sin(\theta) & -c & 0 & 0 & -R_w & 0 & 0 & 0 & 0 & 0\\ \cos(\theta) & \sin(\theta) & c & 0 & 0 & 0 & -R_w & 0 & 0 & 0 & 0\\ \cos(\theta) & \sin(\theta) & -c & 0 & 0 & 0 & 0 & -R_w & 0 & 0 & 0\\ \cos(\theta) & \sin(\theta) & c & 0 & 0 & 0 & 0 & 0 & -R_w & 0 & 0 \end{bmatrix} \quad (75)$$

$$F=\begin{bmatrix}\frac{R_w}{L}(L\cos(\theta+\delta_p)-l\sin(\delta_p+\theta)\sin(\delta_p)) & -l\sin(\delta_p+\theta)\\ \frac{R_w}{L}(L\sin(\theta+\delta_p)+l\cos(\theta+\delta_p)\sin(\delta_p)) & l\cos(\theta+\delta_p)\end{bmatrix}, \quad (88)$$

where $l>0$ is the distance between the look-ahead point and the center of port front wheel and θ is substituted from (83). With this choice of output the determinant of the decoupling matrix F is equal to lR_w and it is everywhere full rank. Therefore, the system is input-output linearizable applying static state feedbacks in (11) and (25).

Proposition 6 (observability)**.** *For the system under study, considering the state space representation in (9) and output in (87), the axial rotation of both front wheels ψ_s, ψ_p along with the summation of the axial rotation of the center wheels $\psi_1+\psi_2$ are locally unobservable at all states.*

Proof: Let $\mathcal{S}$ be a family of nonsingular involutive co-distributions, being invariant under the drift vector field $\mathbf{f}(\mathbf{x})$ and the columns of $G(\mathbf{x})$ in (9) and they contain the span of exact co-vector fields corresponding to the components of the output in (87):

$$\mathcal{G}_0:=\text{span}\{(\frac{\partial \mathbf{y}_1}{\partial \mathbf{x}})^T,(\frac{\partial \mathbf{y}_2}{\partial \mathbf{x}})^T\}. \quad (89)$$

The set of co-distributions $\mathcal{S}$ has a minimal element [32]. We denote the minimal element of $\mathcal{S}$ by $\mathcal{S}_0$ and its involutive annihilator distribution by $\mathcal{S}_0^{\perp}$. At each state $\mathbf{x}_0\in\mathcal{X}$ there is an open neighbourhood $U_0\subset\mathcal{X}$ of $\mathbf{x}_0$ on which the integral of $\mathcal{S}_0^{\perp}$ defines a foliation of largest possible embedded slices with dimension equal to that of $\mathcal{S}_0^{\perp}$ in U_0 containing the unobervable states from the output in (87).

To construct $\mathcal{S}_0$ for the system under study based on (9) and (87), first the co-distribution $\mathcal{G}_0$ is formed. Since $\mathbf{y}$ is only a function of $\mathbf{q}$, the Lie-bracket of any co-vector field in $\mathcal{G}_0$ with respect to columns of $G(\mathbf{x})$ remains in $\mathcal{G}_0$ and hence $\mathcal{G}_0$ is invariant under the columns of $G(\mathbf{x})$. Then, the invariance condition of elements of $\mathcal{S}_0$ under the drift vector field $\mathbf{f}$ is checked. For the first basis element of $\mathcal{G}_0$ this condition results in the co-distribution $\mathcal{G}_1$:

$$\mathcal{G}_1=\mathcal{G}_0+\text{span}\{\mathcal{L}_{\mathbf{f}}(\frac{\partial \mathbf{y}_1}{\partial \mathbf{x}})^T\}, \quad (90)$$

where

$$\mathcal{L}_{\mathbf{f}}(\frac{\partial \mathbf{y}_1}{\partial \mathbf{x}})^T=\mathbf{f}^T(\frac{\partial^2 \mathbf{y}_1}{\partial \mathbf{x}^2})^T+(\frac{\partial \mathbf{y}_1}{\partial \mathbf{x}})^T\frac{\partial \mathbf{f}}{\partial \mathbf{x}}. \quad (91)$$

For the system under study this Lie derivative is calculated using Wolfram Mathematica and the result is a co-vector field that is always traverse to $\mathcal{G}_0$. Therefore, $\mathcal{G}_1$ is of dimension 3. Repeating the same procedure for the second basis element of $\mathcal{G}_0$, we obtain the four dimensional co-distribution $\mathcal{G}_2$:

$$\mathcal{G}_2=\mathcal{G}_1\oplus\text{span}\{\mathcal{L}_{\mathbf{f}}(\frac{\partial \mathbf{y}_2}{\partial \mathbf{x}})^T\}. \quad (92)$$

Based on the normal form in (29), we have at least 4 observable states, i.e., output and its velocity, which is consistent with what we have found so far. Imposing the involutivity condition, the co-distribution $\mathcal{S}_0$ is obtained as the involutive closure of $\mathcal{G}_2$. Calculating $\mathcal{G}_2$ and its involutive closure using Wolfram Mathematica software, the annihilator distribution of $\mathcal{S}_0$ at non-zero velocity states of the system is obtained as

$$\mathcal{S}_0^{\perp}=\begin{bmatrix}0&0&0&1&1&0&0&0&0\\0&0&0&0&0&1&0&0&0\\0&0&1&0&0&0&0&0&0\end{bmatrix}^T. \quad (93)$$

To obtain the unobservable states, the distribution $\mathcal{S}_0^{\perp}$ needs to be integrated. Hence, the unobservable states are $\{\psi_1+\psi_2,\psi_p,\psi_s\}$.

The dimension of the co-distribution $\mathcal{S}_0$ for the system under study based on the state space representation in (9) along with the output in (87), differs at different states of the system. For example, when the system is stationary the dimension of $\mathcal{S}_0$ is 4, i.e., the system contains $9-4=5$ unobservable states (only output and its velocities are observable). However, the maximum dimension of $\mathcal{S}_0$ is 6 indicating that regardless of the state, the system always has at least the 3 unobservable states identified earlier. ■

To construct the normal form state space representation in (31) for the system under study, including the observability decomposition of the internal dynamics, we introduce $\mathbf{z}_1^o=\begin{bmatrix}\theta=\frac{R_w}{2c}(\psi_2-\psi_1) & \delta_p\end{bmatrix}^T$, $\mathbf{z}_1^u=\begin{bmatrix}\psi_2+\psi_1 & \psi_s & \psi_p\end{bmatrix}^T$, and

$$\mathbf{z}_2=\begin{bmatrix}z_6 & z_7 & z_8 & z_9\end{bmatrix}^T:=\begin{bmatrix}\mathbf{y}^T & \dot{\mathbf{y}}^T\end{bmatrix}^T. \quad (94)$$

This set of internal states is selected for simplicity and better indication of the system's performance. It can be verified that this set satisfies the condition in (28) and the resulting state transformation $\mathfrak{T}$ is a diffeomorphism. Accordingly, the functions $\boldsymbol{\omega}^u$ and $\boldsymbol{\omega}^o$ in (31) for the system under study are

$$\boldsymbol{\omega}^u=N^u(\delta_p)F^{-1}\begin{bmatrix}z_8\\z_9\end{bmatrix},\quad \boldsymbol{\omega}^o=\quad N^o(\delta_p)F^{-1}\begin{bmatrix}z_8\\z_9\end{bmatrix}, \quad (95)$$

where

$$N^o=\begin{bmatrix}\frac{R_w\sin(\delta_p)}{L} & 0\\ 0 & 1\end{bmatrix},\ N^u=\begin{bmatrix}\hat{N}_{4,1} & 0\\ \frac{2c}{L}\sin(\delta_p)+2\cos(\delta_p) & 0\\ 1 & 0\end{bmatrix}. \quad (96)$$

The tracking-error zero dynamics corresponding to $\mathbf{z}_1^o$ is formed as:

$$\begin{bmatrix}\dot{\theta}_e & \dot{\delta}_{pe}\end{bmatrix}^T=N^o\begin{bmatrix}z_{8d} & z_{9d}\end{bmatrix}^T F^{-1}-\begin{bmatrix}\dot{\theta}_d & \dot{\delta}_{pd}\end{bmatrix}^T, \quad (97)$$

where θ_e and δ_{pe} respectively refer to the error in θ and δ_p, and z_{8d}, z_{9d}, $\dot{\theta}_d$, and $\dot{\delta}_{pd}$ denote the desired velocities of the output, θ, and δ_p, respectively. Applying Lyapunov's indirect method, it is proved that based on this choice of output for type $(1,1)$ rovers, the tracking-error zero dynamics and consequently the error dynamics of $\mathbf{z}_1^o$ is asymptotically stable, if the system moves in forward direction, and it is unstable during backward motion [30].

Assumption 13. In this paper, we assume that the Lunar autonomous rover only moves in forward direction, and hence $\mathbf{z}_{1e}^o$ is asymptotically stable towards origin.

Remark 12. Since for the Lunar rover the dynamics of $\mathbf{z}_1^u$ in (31) only depends on $\mathbf{z}_1^o$ and $\mathbf{z}_2$, and $\mathbf{z}_{2e}$ and $\mathbf{z}_{1e}^o$ are asymptotically stable due to the proposed output-tracking

control law in (46) and Assumption 13, respectively, the error dynamics $\dot{\mathbf{z}}_{1e}^{u} \to 0$ while $t \to \infty$; and hence $\mathbf{z}_1^u$ is bounded.

For this case study, we consider the following uncertainties in the inertia parameters: (i) an unknown constant mass m_l with a bounded time-varying unknown moment of inertia about the z-axis (out of the plane of motion) $I_{zl}(t)$ that moves with a bounded unknown time varying trajectory $[x_l(t)\ y_l(t)]^T$ in the main body's xy-frame, (ii) an unbalanced port center wheel modeled as an unknown bounded time-varying added m_u to the wheel at an unknown constant radius R_u. In terms of disturbances, we consider an unknown bounded time-varying friction force with the magnitude of $-\varpi_r \text{sgn}(\dot{\theta})$ that is applied on the rear wheels in the lateral direction. Accordingly, the vector of uncertain parameters $\boldsymbol{\rho}$ is formed as: $\boldsymbol{\rho}(t) = \begin{bmatrix} m_l & x_l & y_l & I_{zl} & m_u & R_u & \varpi_r \end{bmatrix}^T$. As the result, the non-zero elements of the matrix $\Delta\hat{M}(\theta, \psi_1, \boldsymbol{\rho})$ are

$$\begin{aligned}
&\Delta\hat{M}_{1,1} = \Delta\hat{M}_{2,2} = m_l + m_u,\\
&\Delta\hat{M}_{1,3} = \Delta\hat{M}_{3,1} = -m_l x_l \sin(\theta) - (cm_u + m_l y_l)\cos(\theta),\\
&\Delta\hat{M}_{1,6} = \Delta\hat{M}_{6,1} = -m_u R_u \sin(\psi_1),\\
&\Delta\hat{M}_{2,3} = \Delta\hat{M}_{3,2} = m_l x_l \cos(\theta) - (cm_u + m_l y_l)\sin(\theta),\\
&\Delta\hat{M}_{3,3} = I_{zl} + c^2 m_u + m_l(x_l^2 + y_l^2),\\
&\Delta\hat{M}_{3,6} = \Delta\hat{M}_{6,3} = cm_u R_u \cos(\theta)\sin(\psi_1),\\
&\Delta\hat{M}_{6,6} = m_u R_u^2.
\end{aligned} \tag{98}$$

The matrix $\Delta\hat{C}(\theta, \psi_1, \boldsymbol{\rho}, \dot{\boldsymbol{\rho}}, \dot{\hat{\mathbf{q}}})$ is then obtained as

$$\Delta\hat{C} = \frac{\partial\Delta\hat{M}}{\partial\theta}\dot{\theta} + \frac{\partial\Delta\hat{M}}{\partial\psi_1}\dot{\psi}_1 + \sum_{i=1}^{7}\frac{\partial\Delta\hat{M}}{\partial\boldsymbol{\rho}_i}\dot{\boldsymbol{\rho}}_i + \begin{bmatrix} \mathbb{O}_{2\times 11} \\ \dot{\hat{\mathbf{q}}}^T\frac{\partial\Delta\hat{M}}{\partial\theta} \\ \mathbb{O}_{2\times 11} \\ \dot{\hat{\mathbf{q}}}^T\frac{\partial\Delta\hat{M}}{\partial\psi_1} \\ \mathbb{O}_{5\times 11} \end{bmatrix}, \tag{99}$$

where $\boldsymbol{\rho}_i$ refers to the i^{th} element of $\boldsymbol{\rho}$. The vector of uncertain potential forces $\Delta\hat{\mathbf{g}}$ due to the unbalanced wheel is

$$\Delta\hat{\mathbf{g}} = \begin{bmatrix} \mathbb{O}_{1\times 5} & -m_u g_u R_u \cos(\psi_1) & \mathbb{O}_{1\times 5} \end{bmatrix}^T, \tag{100}$$

where g_u denotes the gravitational constant. Finally, the direction of the friction disturbance force is determined to be

$$\hat{J}_d = \begin{bmatrix} -\sin(\theta) & \cos(\theta) & -L_0 & \mathbb{O}_{1\times 8} \end{bmatrix}. \tag{101}$$

Subsequent to determining the uncertain matrices $\Delta\hat{M}$ and $\Delta\hat{C}$, the vector $\Delta\hat{\mathbf{g}}$, and the row vector $\hat{J}_d$, the uncertain state-space representation in (35) can be formed for the Lunar autonomous rover and the proposed robust optimal output-tracking control law can be implemented.

A. Simulation Results

The Lunar autonomous rover system along with the proposed controller is modeled in MATLAB R2019b. We discretize our model in (8) with step-time equal to one milisecond and use Euler method for numerical integration. Table I depicts the values of the parameters used in the model of the system, modeled uncertainties, and the controller. A desired trajectory for the rover is considered that includes an acceleration from zero velocities with 0.18m/s^2 in the forward direction of motion for 100s and two steering commands at 10s and 40s. The desired initial value for the vector of generalized coordinates $\hat{\mathbf{q}}$ is set to be $\hat{\mathbf{q}}_d(0) = \begin{bmatrix} -L-l & -c & \mathbb{O}_{1\times 9} \end{bmatrix}^T$, such that the initial value of the desired output trajectory is zero. Following this desired trajectory, the origin of the xy-frame moves on a figure-eight path while it is continuously accelerating (see Fig. 3). Based on (87) the desired trajectory for the output is determined. Note that the designed trajectory has large velocities to highlight the effect of uncertainties at the output. Considering a desired trajectory with low-velocity profile reduces the Coriolis effects of the uncertainties and does not properly reflect the performance of the proposed control law.

Rover Parameters			
L[m]	L_0[m]	c[m]	R_w[m]
1	0.5	0.5	0.3
l[m]	x_{cm}[m]	y_{cm}[m]	m_r[Kg]
1	0.25	0	600
m_w[Kg]	J_r[Kg/m^2]	J_{wy}[Kg/m^2]	J_{wz}[Kg/m^2]
40	450	1.3	1
Uncertain Parameters			
m_l[Kg]	x_l[m]	$\dot{x}_l$[m/s]	y_l[m]
250	$-0.5\cos(t/3)$	$0.16\sin(t/3)$	$0.3\sin(t/3)$
$\dot{y}_l$[m/s]	m_u[Kg]	$\dot{m}_u$[Kg/s]	R_u[m]
$0.1\cos(t/3)$	$0.1-0.025\cos(5t)$	$0.125\sin(5t)$	0.3
I_{zl}[Kg/m^2]	$\dot{I}_{zl}$[Kg/m$^2 s$]	ϖ_r[N]	g_u[m/s^2]
$75-20\cos(t/2)$	$10\sin(t/2)$	140	1.636
Control Parameters			
K_v	K_e	t_f[s]	ϵ_1
$\mathbb{I}_{2\times 2}$	$\mathbb{I}_{2\times 2}$	10	0.31
ϵ_2	κ	β_0	
1	0.55	0.0001	

TABLE I: Kinematic and dynamic parameters of the Lunar rover, uncertain parameters defined in the simulation, and control parameters

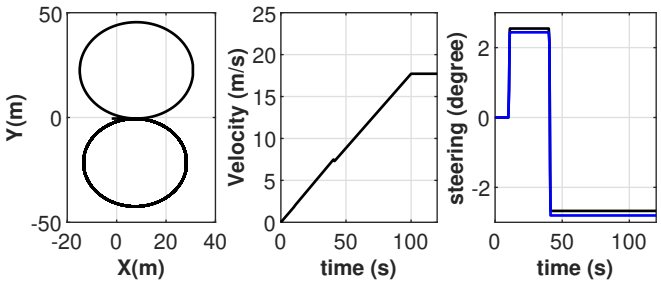

(a) (b) (c)

Fig. 3: Desired trajectory for the rover: (a) desired path (b) desired forward velocity of the rover (c) desired steering angles of port (black line) and starboard (blue line) front wheels

Remark 13. For simplicity, the desired trajectory depicted in Fig.3 is produced based on the commands for quasi-velocities ($\dot{\psi}_p$ and $\dot{\delta}_p$). That justifies the slight reduce in the velocity of the rover at 40^{th} second of the simulation when a considerable change in the steering is applied and system enters another

circle with higher steering angle.

According to the weighting matrices K_v and K_e and the convergence time t_f reported in Table I, the matrix of optimal gains in (58) is obtained as:

$$[K_I^* \;\; K_p^* \;\; K_d^*] = \begin{bmatrix} 0.14 & 0 & 1.19 & 0 & 1.55 & 0 \\ 0 & 0.14 & 0 & 1.19 & 0 & 1.55 \end{bmatrix}.$$

The function β in the switching control law (62) is selected using the equality condition in (61) to be

$$\beta(\mathbf{y}_e) = \frac{\alpha}{1-\sqrt{2}k_0} + \beta_0, \tag{102}$$

where α and k_0 are defined in (59) and (60), respectively. We assume that the rover starts its motion with zero velocity, an initial error $[0 \; 0.5]^T$ in the output, and at the configuration described by $\hat{\mathbf{q}}(0) = \begin{bmatrix} -L-l & -c+0.5 & \mathbb{O}_{1\times 9} \end{bmatrix}^T$. To start the motion of the system on the optimal sliding manifold, we introduce an initial value for the integral of the error, based on (58).

The simulation is once conducted only with the proposed optimal PID control law obtained in (55) as part of the output-tracking SMC design. The results corresponding to this simulation are labeled by "OPID". The same scenario is simulated using the optimal output-tracking SMC with both $\mathbf{v_{eq}}$ in (55) and the switching control law in (72), whose results are labeled by "ORS". The errors in the trajectory tracking for the rover, the output and the steering angles are shown in Fig. 4. Further, the control torques at all wheels and the steering degrees of freedom are compared in Fig. 5.

Based on Fig. 4 in both control approaches, system is navigated from its initial location towards the desired trajectory and tracks it with an acceptable amount of error caused by the imposed uncertainties and disturbances. By acceptable error we mean less than half a meter maximum magnitude of the steady state error in the position of the rover during circling with a high velocity equal to $17.5m/s$. Since in the design of the optimal controller t_f is $10s$, the control system is in the steady state regime after $t = 10s$. However, it is evident that adding the proposed switching control law improves the robustness of the controller and reduces the error by one order of magnitude (from near 0.2m to near 2cm). Considering Fig. 4c and Fig. 4d, the output converges to its desired trajectory almost at the prescribed time of $t_f = 10$s, while according to Fig. 4a and Fig. 4b the rover reaches its prescribed trajectory slightly after 10s. In addition since the controllers were designed to regulate the system output, it is observed from Fig. 4 that the magnitude of the error in the rover motion is marginally more than that of the output, throughout the simulation. This difference is directly influenced by the location of the look-ahead point. The system particularly demonstrate non-minimum phase behaviour due to its nonholonomicity in the first 10s of its motion, where the controller attempts to zero the error in $\mathbf{y}_2$ in the expense of introducing considerable errors in x_b and steering angles. It is also noted that the effects of uncertainties at the output are directly correlated with the amount of the rover acceleration and its velocity, due to the appearance of uncertainties in the mass matrix and the Coriolis and Centrifugal terms. This is

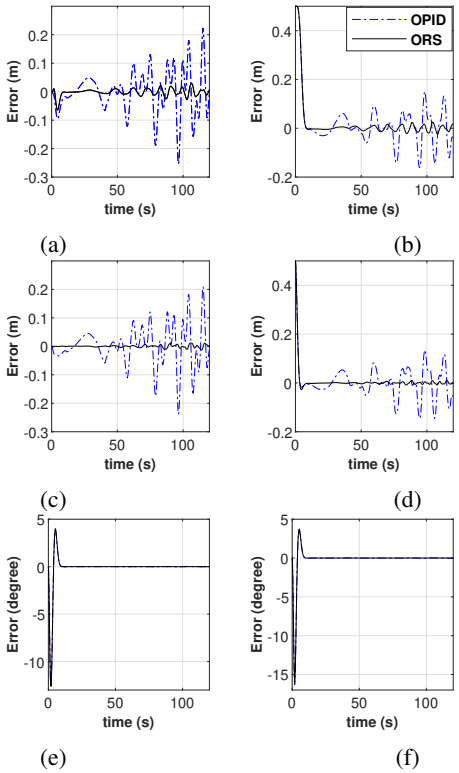

Fig. 4: Performance comparison of OPID and ORS in terms of error in (a) x_b, (b) y_b, (c) y_1, (d) y_2, (e) δ_p, and (f) δ_s

the reason behind the observed increase in the error in Fig. 4 as the time elapses.

According to Fig. 5, the control actions produced by the ORS control scheme follow the same trend comparing with those obtained in the OPID case, with the addition of some chattering effects as the result of the proposed switching control law. The magnitude of the chattering can be adjusted by a proper choice of the variable κ. Generally, smaller κ results in smaller magnitude of errors but larger amplitude of chartering in control actions. Based on the adjusted variable for κ (see Table I), the highest amplitude of chattering is observed to be near 5N.m. When the system moves with a constant velocity (after time 100s) on a circle since the center of mass is located ahead of the origin of the xy-frame, both controllers are producing time-varying brake forces to compensate for the Coriolis effects. The low-frequency oscillations (with large amplitude) in the produced control actions by both control laws during circling are due to the sinusoidal changes in the location of the center of mass of the system. Throughout the motion, the system also experiences high-frequency oscillations (with small amplitude) in the produced control torques as the result of the unbalanced port center wheel. The period of the high-frequency oscillations decreases as the velocity of the system increases.

VI. Conclusion

In this paper, mechanical systems subject to mixed holonomic and nonholonomic constraints in Pfaffian form were studied from various control perspectives, including reachability, feedback linearizability , and observability. Under

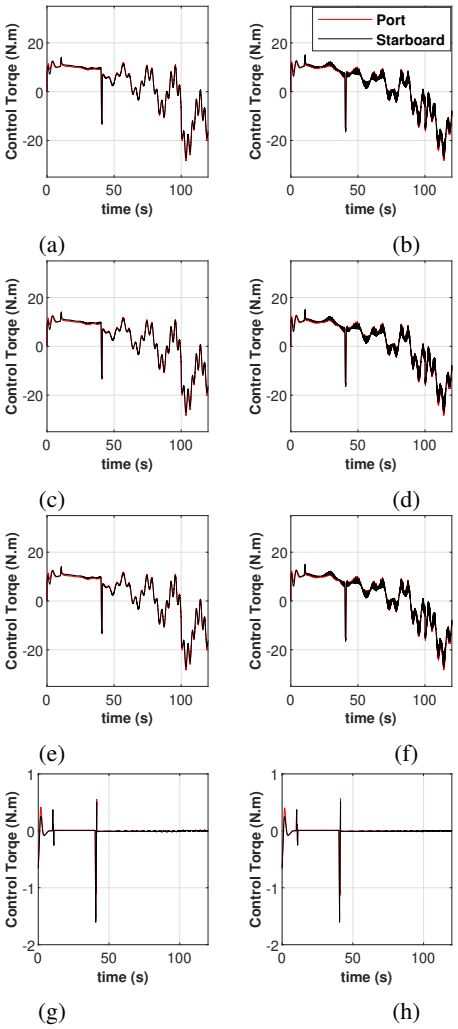

Fig. 5: Comparison of control commands generated by OPID (left) and ORS (right) laws. From the top to the bottom row, the plots respectively correspond to torques at the front wheels, center wheels, rear wheels, and steering degrees of freedom.

some conditions, the input-output linearization of such systems applying static state feedback was presented. Accordingly, we partitioned the states of the system into external states, and observable and unobservable internal states from the output of the control system before applying the linearizing feedback transformation. Such a partitioning of the states helps investigate the stability of the tracking error of the internal states that was demonstrated in the implementation phase. Including time-dependant bounded matched uncertainties in the inertia parameters and disturbance forces, the uncertain state-space representation of constrained mechanical systems was formulated. Applying the input-output linearizing feedback to the nominal plant, an output-tracking SMC algorithm was developed. We proposed an optimal design for the sliding manifold based on the finite-horizon LQR problem with splitting boundary value conditions. We also improved the performance of the switching control law in the optimal SMC by substituting the sign function with a high-slope saturation function and discussed its implications on the system's error dynamics. The developed control law was used in the output-tracking control of a six-wheel autonomous Lunar rover, in a simulation environment. The results were compared with those obtained using the optimal PID control strategy. We showed that although the optimal PID demonstrated an acceptable performance in terms of both error and control actions, the addition of the proposed switching control law improved the error performance by one order of magnitude without considerably affecting the control actions.

Some possible future directions of this research are: (i) studying optimal distribution of the control actions when lifted to the unrestricted manifold, considering, e.g., traction of rover systems, and (ii) investigating the effects of violation of constraints, e.g., wheel slip in rovers, in the robust control design process.

APPENDIX I
A_L AND B_L MATRICES

The nonzero elements of the constant matrix A_L in (52) are:

$$\begin{aligned}
&A_{L1,3} = A_{L2,4} = A_{L3,5} = A_{L4,6} = 1,\\
&A_{L5,11} = -\frac{1}{K_{v1,1}}, \quad A_{L6,12} = -\frac{1}{K_{v2,2}},\\
&A_{L9,3} = -K_{e1,1}, \quad A_{L10,4} = -K_{e2,2},\\
&A_{L9,7} = A_{L10,8} = A_{L11,9} = A_{L12,10} = -1,
\end{aligned}$$

where $A_{Li,j}$ refers to the element (i,j) of the matrix A_L, $K_{vi,j}$ denotes the element (i,j) of the weighting matrix K_v, and $K_{ei,j}$ denotes the element (i,j) of the weighting matrix K_e. Choosing the weighting matrices K_v and K_e as the identity matrix, and selecting $t_f = 10s$ the determinant of the matrix $B_{Lf1,2}$ is 1.54×10^{12}; and hence this matrix is well-conditioned.

APPENDIX II
$\hat{M}$ AND $\hat{C}$ MATRICES

The nonzero elements of the matrix $\hat{M}$ are:

$$\begin{aligned}
&\hat{M}_{1,1} = \hat{M}_{2,2} = m_r + 6m_w,\\
&\hat{M}_{1,3} = \hat{M}_{3,1} = (2(L_0 - L)m_w - x_{cm}m_r)\sin(\theta) - y_{cm}m_r\cos(\theta),\\
&\hat{M}_{2,3} = \hat{M}_{3,2} = 2m_w(L - L_0)\cos(\theta) + m_r(x_{cm}\cos(\theta) - y_{cm}\sin(\theta)),\\
&\hat{M}_{3,3} = 6(m_w c^2 + J_{wz}) + 2m_w(L^2 + L_0^2) + m_r(x_{cm}^2 + y_{cm}^2 + J_r,\\
&\hat{M}_{3,5} = \hat{M}_{5,3} = \hat{M}_{3,11} = \hat{M}_{11,3} = \hat{M}_{5,5} = \hat{M}_{11,11} = J_{wz},\\
&\hat{M}_{4,4} = \hat{M}_{6,6} = \cdots = \hat{M}_{10,10} = J_{wy},
\end{aligned}$$

where m_r is the mass of the main body, m_w is the mass of the wheels, J_r is the moment of inertia of the main body about the z-axis (out of the plane) at its center of mass, J_{wy} denotes the moment of inertia of the wheels about their axes of rotation, and J_{wz} is the the moment of inertia of the wheels about the z_0-axis. Accordingly, based on the Lagrange d'Alembert principle, the matrix $\hat{C}$ is obtained as

$$\hat{C}(\theta, \dot{\hat{\mathbf{q}}}) = (\frac{\partial \hat{M}}{\partial \theta})\dot{\theta} + \begin{bmatrix} \mathbb{O}_{11\times 2} & \frac{1}{2}(\dot{\hat{\mathbf{q}}}^T \frac{\partial \hat{M}}{\partial \theta})^T & \mathbb{O}_{11\times 8} \end{bmatrix}^T.$$

REFERENCES

[1] B. He, S. Wang, and Y. Liu, "Underactuated robotics: a review," *International Journal of Advanced Robotic Systems*, vol. 16, no. 4, p. 1729881419862164, 2019.

[2] R. M. Murray, Z. Li, S. S. Sastry, and S. S. Sastry, *A mathematical introduction to robotic manipulation*. CRC press, 1994.

[3] B. Siciliano, L. Sciavicco, L. Villani, and G. Oriolo, *Robotics: modelling, planning and control*. Springer Science & Business Media, 2010.

[4] J. Kovecses, J.-C. Piedboeuf, and C. Lange, "Dynamics modeling and simulation of constrained robotic systems," *IEEE/ASME Transactions on mechatronics*, vol. 8, no. 2, pp. 165–177, 2003.

[5] X. Yun and N. Sarkar, "Unified formulation of robotic systems with holonomic and nonholonomic constraints," *IEEE Transactions on Robotics and Automation*, vol. 14, no. 4, pp. 640–650, 1998.

[6] I. Kolmanovsky and N. McClamroch, "Developments in nonholonomic control problems," *IEEE Control Systems Magazine*, vol. 15, no. 6, pp. 20–36, 1995.

[7] A. Bloch and N. McClamroch, "Control of mechanical systems with classical nonholonomic constraints," in *Proceedings of the 28th IEEE Conference on Decision and Control,*, 1989, pp. 201–205 vol.1.

[8] A. M. Bloch, "Nonholonomic mechanics and control." Springer, 2003.

[9] I. I. Hussein and A. M. Bloch, "Optimal control of underactuated nonholonomic mechanical systems," *IEEE Transactions on Automatic Control*, vol. 53, no. 3, pp. 668–682, 2008.

[10] G. Walsh, D. Tilbury, S. Sastry, R. Murray, and J. Laumond, "Stabilization of trajectories for systems with nonholonomic constraints," *IEEE Transactions on Automatic Control*, vol. 39, 1994.

[11] L. J. Colombo, D. M. de Diego, A. Nayak, and R. T. Sato Martin de Almagro, "Geometric optimal trajectory tracking of nonholonomic mechanical systems," *SIAM Journal on Control and Optimization*, vol. 58, no. 3, pp. 1652–1675, 2020.

[12] N. Sarkar, X. Yun, and V. Kumar, "Control of mechanical systems with rolling constraints: Application to dynamic control of mobile robots," *The International Journal of Robotics Research*, vol. 13, no. 1, pp. 55–69, 1994.

[13] R. Chhabra and M. R. Emami, "A unified approach to input-output linearization and concurrent control of underactuated open-chain multibody systems with holonomic and nonholonomic constraints," *Journal of Dynamical and Control Systems*, vol. 22, pp. 129–168, 2016.

[14] R. Chhabra, M. R. Emami, and Y. Karshon, "Reduction of hamiltonian mechanical systems with affine constraints: A geometric unification," *Journal of Computational and Nonlinear Dynamics*, vol. 12, no. 2, 2017.

[15] R. Chhabra, "Dynamical reduction and output-tracking control of the lunar exploration light rover (lelr)," in *2016 IEEE Aerospace Conference*. IEEE, 2016, pp. 1–8.

[16] H. K. Khalil and J. W. Grizzle, *Nonlinear systems*. Prentice hall Upper Saddle River, NJ, 2002, vol. 3.

[17] L. Le-Tien and A. Albu-Schäffer, "Robust adaptive tracking control based on state feedback controller with integrator terms for elastic joint robots with uncertain parameters," *IEEE Transactions on Control Systems Technology*, vol. 26, no. 6, pp. 2259–2267, 2018.

[18] M. Souzanchi-K., A. Arab, M.-R. Akbarzadeh-T., and M. M. Fateh, "Robust impedance control of uncertain mobile manipulators using time-delay compensation," *IEEE Transactions on Control Systems Technology*, vol. 26, no. 6, pp. 1942–1953, 2018.

[19] S. Gambhire, D. R. Kishore, P. Londhe, and S. Pawar, "Review of sliding mode based control techniques for control system applications," *International Journal of Dynamics and Control*, vol. 9, pp. 363–378, 2021.

[20] Y. Xu, "Chattering free robust control for nonlinear systems," *IEEE Transactions on Control Systems Technology*, vol. 16, no. 6, pp. 1352–1359, 2008.

[21] E. Tahoumi, F. Plestan, M. Ghanes, and J.-P. Barbot, "New robust control schemes based on both linear and sliding mode approaches: Design and application to an electropneumatic actuator," *IEEE Transactions on Control Systems Technology*, 2019.

[22] S. S. Ge, Z. Wang, and T. H. Lee, "Adaptive stabilization of uncertain nonholonomic systems by state and output feedback," *Automatica*, vol. 39, no. 8, pp. 1451–1460, 2003.

[23] Z. Wang, S. Ge, and T. Lee, "Robust motion/force control of uncertain holonomic/nonholonomic mechanical systems," *IEEE/ASME Transactions on Mechatronics*, vol. 9, no. 1, pp. 118–123, 2004.

[24] Y. Hu, S. Ge, and C.-Y. Su, "Stabilization of uncertain nonholonomic systems via time-varying sliding mode control," *IEEE Transactions on Automatic Control*, vol. 49, no. 5, pp. 757–763, 2004.

[25] J. Zakrajsek, D. McKissock, J. Woytach, J. Zakrajsek, F. Oswald, K. McEntire, G. Hill, P. Abel, D. Eichenberg, and T. Goodnight, "Exploration rover concepts and development challenges," in *1st Space Exploration Conference: Continuing the Voyage of Discovery*, 2005, p. 2525.

[26] Y. Kanayama, Y. Kimura, F. Miyazaki, and T. Noguchi, "A stable tracking control method for an autonomous mobile robot," in *Proceedings., IEEE International Conference on Robotics and Automation*. IEEE, 1990, pp. 384–389.

[27] J.-M. Yang and J.-H. Kim, "Sliding mode control for trajectory tracking of nonholonomic wheeled mobile robots," *IEEE Transactions on robotics and automation*, vol. 15, no. 3, pp. 578–587, 1999.

[28] H. Ashrafiuon, S. Nersesov, and G. Clayton, "Trajectory tracking control of planar underactuated vehicles," *IEEE transactions on automatic control*, vol. 62, no. 4, pp. 1959–1965, 2016.

[29] B. d'Andréa Novel, G. Campion, and G. Bastin, "Control of nonholonomic wheeled mobile robots by state feedback linearization," *The International journal of robotics research*, vol. 14, no. 6, pp. 543–559, 1995.

[30] D. Wang and G. Xu, "Full-state tracking and internal dynamics of nonholonomic wheeled mobile robots," *IEEE/ASME Transactions on mechatronics*, vol. 8, no. 2, pp. 203–214, 2003.

[31] X. Yun and Y. Yamamoto, "Stability analysis of the internal dynamics of a wheeled mobile robot," *Journal of Robotic Systems*, vol. 14, no. 10, pp. 697–709, 1997.

[32] A. Isidori, *Nonlinear control systems*. Springer Science & Business Media, 2013.

[33] J.-J. E. Slotine, W. Li *et al.*, *Applied nonlinear control*. Prentice hall Englewood Cliffs, NJ, 1991, vol. 199, no. 1.

[34] R. Hermann and A. Krener, "Nonlinear controllability and observability," *IEEE Transactions on automatic control*, vol. 22, no. 5, pp. 728–740, 1977.

[35] H. Nijmeijer and A. J. Van der Schaft, *Nonlinear dynamical control systems*. Springer, 1990, vol. 175.

[36] D. E. Kirk, *Optimal control theory: an introduction*. Courier Corporation, 2004.

[37] G. Campion, G. Bastin, and B. Dandrea-Novel, "Structural properties and classification of kinematic and dynamic models of wheeled mobile robots," *IEEE Transactions on Robotics and Automation*, vol. 12, no. 1, pp. 47–62, 1996.

M.R Mottaghi was born in Esfahan, Esfahan, Iran in 1996. He received the B.S. degree in mechanical engineering from Isfahan University of Technology,Esfahan, Iran, in 2019. Then, he joined Autonomous Space Robotics and Mechatronics Lab (ASRoM Lab) at Carleton University, Ottawa, ON, Canada to pursue his M.A.Sc degree in mechanical engineering in 2019. Since 2019, he has been working as a Research Assistant with ASRoM Lab. His research interests include, robust control design, nonholonomic mechanics and control, and traction control for autonomous rovers.

Robin Chhabra (IEEE Member) is a Tier-II Canada Research Chair in autonomous space robotics and mechatronics at Carleton University. His team is focused on developing methodologies for the long-term, intelligent autonomy of space robotic systems. Dr. Chhabra received his M.A.Sc. (2008) and Ph.D. (2013) from the University of Toronto Institute for Aerospace Studies. After a postdoctoral fellowship at the University of Calgary, he joined MacDonald Dettwiler and Associates Ltd., where he focused on applied research on the control of space systems. Dr. Chhabra's research interest include applications of geometric mechanics, nonlinear controls, and artificial intelligence, in the control of robotic systems.